Separation and Purification Technology 353 (2025) 128436

Contents lists available at ScienceDirect

Separation and Purification Technology

journal homepage: www.elsevier.com/locate/seppur

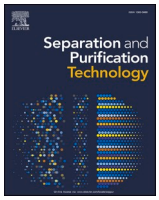

Synergistic effect of Fe and Ni on carbon aerogel for enhanced oxygen reduction and H_2O_2 activation in electro-Fenton process

Qian Ye [a], Timothy N. Hunter [b,*], Hao Xu [c], David Harbottle [b], Girish M. Kale [b], Martin R. Tillotson [a,*]

[a] School of Civil Engineering, University of Leeds, Leeds LS2 9JT, UK
[b] School of Chemical and Process Engineering, University of Leeds, Leeds LS2 9JT, UK
[c] Environment and Sustainability Institute, Faculty of Environment, Science and Economy, University of Exeter, Penryn Campus, Penryn TR10 9FE, UK

ARTICLE INFO

Editor: Shujuan Zhang

Keywords:
FeNi alloy
Carbon aerogel
Electro-Fenton technology
Oxygen reduction reaction
Organic contaminant

ABSTRACT

A novel cathode, iron-nickel alloy modified carbon aerogel (FeNi-CA), was successfully synthesized and utilized as the cathode in an electro-Fenton process for acetaminophen degradation. The incorporation of Fe and Ni in the carbon matrix resulted in superior electrochemical characteristics and catalytic performance compared to Fe-CA and Ni-CA. The unique microstructure of FeNi-CA, including the presence of alloy nanoparticles, carbon defects, and abundant oxygen functional groups, enhanced $2e^-$ oxygen reduction activity and electrocatalytic performance. This enabled FeNi-CA to exhibit a dual functionality of H_2O_2 electro-generation and *in situ* activation. FeNi-CA demonstrated good performance over a wide pH range at a low current density of 4.44 mA/cm^2. Under optimal conditions, 99.9 % of acetaminophen was removed with a reaction rate constant (k_{obs}) of 0.054 min^{-1} through electro-sorption and oxidation processes. Importantly, a satisfactory degradation effect was achieved in the absence of external aeration. This work provides a potential wastewater treatment solution without the need for external aeration or additional chemical input by simultaneously achieving oxygen evolution reaction at the anode and oxygen reduction reaction at the cathode. Furthermore, FeNi-CA demonstrated good reusability performance with controlled metal leaching after five consecutive runs, suggesting its potential for sustained use in electro-Fenton processes over the long term.

1. Introduction

The presence of pharmaceutical compounds, representing the most substantial category of emerging micropollutants, has raised significant public health concerns because of their existence in various environmental compartments [1]. Acetaminophen (ACT) is one of the most commonly reported pharmaceutical products currently found in water resources [2,3], with significant adverse effects on human health, potentially leading to antibiotic resistance, endocrine disruption, and various chronic diseases [4]. Thus, ACT has emerged as a significant challenge for the treatment of domestic wastewater.

Solar photolysis, biodegradation, and conventional treatment methods such as activated sludge processes with adsorption, sedimentation, and filtration using membranes are generally inadequate for the comprehensive removal of ACT [5]. As an alternative, advanced oxidation processes (AOPs) are chemical methods that involve the activation of certain molecules (e.g., hydrogen peroxide, ozone, persulfate), leading to the production of highly reactive radicals such as hydroxyl radicals and sulfate radicals [6]. These radicals engage in rapid and non-selective reactions with organic contaminants including ACT, ultimately breaking them down into harmless smaller molecules and achieving the purification of wastewater [7]. Nevertheless, despite significant advancements in AOPs since their formal introduction in 1987 by Glaze et al. [8], two primary challenges continue to restrict their widespread application. The first challenge associated with AOPs is the efficient activation of hydrogen peroxide (H_2O_2). In commercialized AOPs, ultraviolet light is commonly employed to produce hydroxyl radicals ($^{\bullet}OH$) by cleaving the O-O bond in H_2O_2 [9]. However, this process is highly energy-intensive. The second challenge is the sustainable production of H_2O_2. The current industrial method, known as the anthraquinone process, demands complex infrastructure and is impractical for small-scale applications [10]. Additionally, the risks related to the transportation and storage of H_2O_2 pose further obstacles to applying AOPs in remote locations and isolated communities [11].

* Corresponding authors.
E-mail addresses: T.N.Hunter@leeds.ac.uk (T.N. Hunter), M.R.Tillotson@leeds.ac.uk (M.R. Tillotson).

https://doi.org/10.1016/j.seppur.2024.128436
Received 29 March 2024; Received in revised form 4 June 2024; Accepted 13 June 2024
Available online 16 June 2024

Electro-Fenton (EF) technology, as one of the most promising AOPs, has the potential to generate H_2O_2 on-site and activate it under mild conditions. Besides, it has the advantages of a relatively simple reaction device and the elimination of the need for additional oxidants [12,13]. At the cathode in EF processes, oxygen undergoes a two-electron reduction reaction ($2e^-$ ORR), resulting in the generation of H_2O_2 as shown in Eq. (1) [14]. The produced H_2O_2 then reacts with an electro-Fenton catalyst, leading to the generation of highly reactive species such as $^{\bullet}OH$ [15].

$$O_2 + 2H^+ + 2e^- \rightarrow H_2O_2 \quad (1)$$

The key processes in EF technology involve the generation and activation of H_2O_2. The efficiency of H_2O_2 generation depends on the characteristics of the cathodic material. Carbon-based materials such as graphite felt (GF) [16,17], carbon nanotubes (CNT) [18], amorphous carbon black (CB) [19,20], and carbon aerogel (CA) [21] are commonly used in the cathodic matrix. Among them, CA is an outstanding candidate for cathode material and metal support because of its good electrical conductivity, large surface area, and corrosion resistance [22]. In recent studies, diverse approaches have been explored to enhance the electrochemical production of H_2O_2 using modified carbon materials [23–25]. These have highlighted the significance of both the quantity and type of oxygenated surface functional groups [26]. For instance, a higher concentration of carboxyl groups leads to enhanced efficiency in generating H_2O_2 [27]. Furthermore, carbon-based materials with a higher disordered carbon ratio exhibit increased H_2O_2 production [28]. In general, carbonaceous materials with some significant features such as extensive surface area, C═C bonds, and the existence of oxygenated groups have been shown to exhibit higher catalytic activity for $2e^-$ ORR to produce H_2O_2 [26], which offers guidance for modifying carbon-based materials to enhance the yield of H_2O_2.

Due to its limited oxidation capacity, H_2O_2 alone is not active enough for the degradation of most pollutants thus highlighting the importance of the activation process for H_2O_2. In homogeneous EF processes, H_2O_2 can be activated using an externally added catalyst (Fe^{2+}) according to the Fenton reaction in Eq. (2). However, this presents challenges in a limited pH application range because of the formation of iron sludge [29]. In contrast, solid catalysts are employed in the heterogeneous EF processes, thus extending the pH range and addressing the limitations of homogeneous EF technology [30,31]. Among heterogeneous EF catalysts in previous studies, the applications of cathodes with assembled active Fe components hold significant importance for the electrocatalytic decomposition of contaminants. For example, a gas diffusion electrode (GDE) with the immobilization of active Fe_3O_4 as a rotating cathode was found to be capable of decomposing H_2O_2 into $^{\bullet}OH$ [32]. Similarly, Cui et al. [33] developed a Fe_3O_4/MWCNTs/CB (carbon black) GDE, which demonstrated exceptional performance in the activation of H_2O_2. However, carbon catalysts doped with iron exhibit exceptional activity in the $4e^-$ ORR, leading to a reduced yield of H_2O_2 [34]. Therefore, enhancing the selectivity for the $2e^-$ ORR is crucial for Fe-based integrated cathodes to effectively produce $^{\bullet}OH$ radicals. Compared to monometallic Fe/carbon composite catalysts, bimetallic carbon composite catalysts possess the potential to enhance the overall efficiency of the catalysts [35]. These composites, comprising various species working synergistically, not only optimize the electronic structure but also enhance the charge-carrier density and improve conductivity [36]. Among these bimetallic materials, Fe-Ni mixture exhibits significant electrocatalytic activity [37]. The introduction of Ni is expected to enhance the $2e^-$ selectivity of Fe-based cathodes for the oxygen reduction reaction. To the best of our knowledge, there are currently no studies on the composite of FeNi active sites and carbon aerogel as a cathode for EF system. The synergistic effects of Fe and Ni on the configuration and electrochemical characteristics of carbon aerogel (CA) have not been revealed.

$$Fe^{2+} + H_2O_2 \rightarrow Fe^{3+} + OH^- + \bullet OH \quad (2)$$

Furthermore, previously reported EF processes usually require oxygen/compressed air sparging to enhance H_2O_2 production [38,39]. However, the oxygen utilization efficiency was found to be less than 0.1 % [40], indicating that a significant portion of the oxygen was not effectively utilized for H_2O_2 production and therefore caused a high cost. Hence, the development of an Electro-Fenton system that requires less oxygen or even eliminates the need for external oxygen input would be both economically advantageous and hold great promise for practical applications.

Herein, a new heterogeneous EF system was established using FeNi alloy carbon aerogel (FeNi-CA) as the cathode to achieve simultaneous generation and *in situ* activation of H_2O_2 without the need for external aeration. The microstructures and chemical compositions of the as-synthesized Fe-CA, Ni-CA, and FeNi-CA were analyzed and compared using characterization techniques. The synergistic effects of Fe and Ni on carbon aerogel for enhanced ORR activity and selectivity were evaluated in detail. We also assessed the performances of the EF system for the decomposition of ACT. The impacts of various reaction parameters, including initial pH, current, and aeration rate were also investigated. Furthermore, potential mechanisms of radical generation and ACT degradation pathways were proposed. The innovative process proposed in this work ensures the efficient production and immediate activation of H_2O_2 directly on the cathode surface, offering new insights for the development of novel heterogeneous EF systems and enhancing the efficiency of removing micropollutants.

2. Materials and methods

Information about chemicals and reagents, cathode characterization, analytical methods, and electrochemical tests are provided in the Experimental Section of the Electronic Supplementary Materials (ESM).

2.1. Cathode synthesis

The synthesis of single and alloy metal carbon aerogel cathodes in this research involved the following steps: (I) gelation phase, involving the creation and reinforcement of the gel through sol–gel and aging processes; (II) solvent exchange of water in the obtained wet gel structure with acetone; (III) drying, for the formation of the aerogel through drying the gel at room temperature and pressure; and (IV) carbonization, the acquisition of the final aerogel through carbonization at high temperature in a continuous flow of N_2.

Synthesis steps for the iron-nickel carbon aerogel (FeNi-CA) are similar to the method reported by Xiao et al. [41]. Firstly, 11.011 g of resorcinol was mixed with 19.64 mL of Milli-Q water. Then, 15 mL of formaldehyde (37 %) and 0.0085 g of sodium carbonate were added to the mixture under constant stirring until completely dissolved. Subsequently, the metallic precursors for FeNi-CA i.e., ferric acetylacetonate (0.5375 g) and nickel acetylacetonate (0.3721 g) respectively, were dissolved in the homogeneous solution. Since the molar ratio of Fe:Ni is 1:1 at this dosage, this cathode was also marked as $Fe_{0.5}Ni_{0.5}$-CA. After one hour of magnetic stirring, the mixture was poured into a cuboid Teflon mold. The well-sealed Teflon mold containing the precursor solution was cured in an oven using a stepped temperature profile (30 °C for 24 h, 50 °C for 24 h, and 90 °C for 72 h) to complete the polymerization and aging processes. An example of the obtained wet-gel in the mold is presented within the Electronic Supplementary Materials (ESM, Fig. S1 (a)). Subsequently, the obtained wet gel was completely immersed in acetone for 72 h to thoroughly replace the water remaining in the carbon structure, before drying under ambient conditions for one day. Acetone was chosen as the exchange solvent because of its lower surface tension to reduce the shrinkage of the gel [42]. Finally, the molded aerogel was calcined in a tube furnace (Carbolite Gero TZF 12/38) under N_2 atmosphere with a flow rate of 0.1 L/min. The heating rate was set at 3 °C/min, starting from room temperature and reaching 950 °C, where it was maintained for 4 h. After the carbonization

procedure, the obtained FeNi-CA was cooled to ambient temperature and used as the integrated cathode in the electro-Fenton system. The obtained FeNi-CA cathode is also shown within the ESM (Fig. S1 (b)).

Similar procedures were also used to synthesize the single metal iron carbon aerogel (Fe-CA) and nickel carbon aerogel (Ni-CA), with the addition of 0.5375 g of ferric acetylacetonate and 0.3721 g of nickel acetylacetonate, respectively. The metal precursors for $Fe_{0.7}Ni_{0.3}$-CA were 0.7525 g ferric acetylacetonate and 0.2233 g nickel acetylacetonate, and for $Fe_{0.3}Ni_{0.7}$-CA were 0.3225 g ferric acetylacetonate and 0.5209 g nickel acetylacetonate.

2.2. Electrochemical degradation

Electrocatalytic degradation experiments were carried out in a 150 mL single-chamber cylindrical glass cell. The fabricated carbon aerogels (working area of 4.5 cm^2) and platinum sheet (working area of 4.0 cm^2) functioned as cathode and anode, respectively. The distance between the two electrodes was kept at 2 cm. In most experiments, the DC power supply (Velleman 70–0768) was set at the optimal operative current of 20 mA for the electrocatalytic degradation process, and the relevant potential was monitored as 1.5–2.7 V. In electro-sorption (ES) experiments, the current was kept at 1 mA under 0.2 L/min N_2 atmosphere with a relevant potential of 1.3–1.5 V. The pH of the solution was adjusted with H_2SO_4 (0.1 mol/L) and NaOH (0.1 mol/L) to the desired value. Dissolved oxygen concentration and pH values were measured using HQ 40d (Hach, UK) digital multi-meter kit. The reaction was initiated by aeration with compressed air at a predetermined flow rate into the simulated wastewater, which consisted of 0.05 mol/L Na_2SO_4 and 10 mg/L ACT. Samples for analysis were collected at predetermined intervals and then filtered using a 0.22 μm syringe filter. The concentration of ACT was quantified using high-performance liquid chromatography (HPLC), with details are provided in the ESM. The electrochemical degradation of ACT was described using the pseudo-first-order kinetic model, represented using Eq. (3) [43]:

$$ln(C_0/C_t) = k_{obs}t \tag{3}$$

where k_{obs} is the apparent reaction rate constant (min^{-1}), t is the reaction time (min), and C_0 and C_t represent the initial ACT concentration (mg/L) and ACT concentration at time t (mg/L), respectively.

Electrical energy consumptions and costs in the electro-Fenton process were calculated according to Eq. (4) [44]:

$$EC_{ACT}\left(kWh/kg_{ACT}\right) = I \bullet V \bullet t/\Delta m_{ACT} \tag{4}$$

where EC_{ACT} (kWh/kg_{ACT}) is the energy consumption per degraded ACT mass, I is the applied current (A), V is the average voltage (V), t is the treatment time (h), Δm_{ACT} is the ACT mass removal (g).

The synergistic effect (SE) was determined according to Eq. (5) [45] by evaluating the efficiency of pollutant removal in the bimetallic process against the total efficiencies of each sole process:

$$SE = \left(\frac{k_{FeNi-CA}}{k_{Fe-CA} + k_{Ni-CA}} - 1\right)*100 \tag{5}$$

where $k_{FeNi\text{-}CA}$, $k_{Fe\text{-}CA}$, and $k_{Ni\text{-}CA}$ represent the rate constants of the FeNi-CA process, Fe-CA, and Ni-CA process, respectively.

The cyclic experiments were conducted by collecting and washing the used cathode with Milli-Q^{TM} water (Merk Millipore) and then employing it for subsequent repeated runs under identical experimental conditions. The electrocatalytic stability and recyclability of the cathodes were evaluated through the degradation efficiency of ACT over the reused cathode.

3. Results and discussion

3.1. Surface and structural properties

X-ray diffraction (XRD) analysis was conducted to demonstrate the composition and crystal structure of the synthesized FeNi-CA, Fe-CA and Ni-CA cathodes, as shown in Fig. 1 (a). Two broad XRD diffraction peaks at 23.3° for FeNi-CA and Ni-CA are observed, corresponding to the (002) reflection of the graphitic carbon [46,47]. This peak becomes sharper and shifts slightly to 25.9° in the Fe-CA cathode sample, and a small peak at 43.2° appears, which may be ascribed to amorphous carbon [34,47]. The XRD pattern of Ni-CA shows three sharp peaks at 44.5°, 51.9°, and 76.6° (2θ), which can be indexed to the three reflections of (111), (200) and (220) crystal planes of cubic Ni according to the JCPDS No. 04-0850 [48]. Besides, an obvious diffraction peak of Ni-CA at 29.5° is observed for NiC_x (JCPDS No. 45-0979) [49]. The crystalline phase of iron in Fe-CA is composed of zero valence state Fe^0 (110) and oxidation state Fe_3O_4 (JCPDS 89-0951) [50], and the minor peaks detected for Fe_3O_4 are preserved in the FeNi-CA cathode. Previous studies have shown that Fe_3O_4 has the ability to catalyze the decomposition of H_2O_2 to produce $^{\bullet}OH$ [51], which can contribute to the heterogeneous Fenton reaction. Furthermore, the XRD spectrum of FeNi-CA shows a good crystalline structure of $FeNi_3$ as evidenced by three diffraction peaks located at 43.9°, 51.2°, and 75.2° corresponding to (111), (200), (220) crystal facets from the face-centered-cubic $FeNi_3$ phase (JCPDS, No. 65-3244) [47]. These XRD results revealed the formation of $FeNi_3$ alloy and graphitic carbon phases in the synthesized FeNi-CA cathode.

The porosity of the FeNi-CA, Fe-CA, and Ni-CA was further investigated with N_2 adsorption–desorption isotherms, as illustrated in Fig. 1 (b). All cathodes exhibit an isotherm categorized as IUPAC Type IV with an H1 hysteresis loop, reflecting their prominent mesoporous structures [52]. Additionally, the comparison of the pore structures between CA and FeNi-CA in Fig. S2 indicated that the prominent mesoporous structure of CA doesn't change after depositing FeNi alloy, while the smaller pores may be filled or covered by the FeNi alloy particles. At a low relative pressure of $P/P_0 = 0.1$, the observed adsorption suggests the existence of micropores. Conversely, at higher relative pressures, the adsorption indicates the presence of mesopores in FeNi-CA [53]. Micropores offer abundant active sites for the oxygen reduction reaction, while meso-macro pores act as gas transfer pathways, supplying oxygen and enabling the electrolyte to permeate into the cathode interior. This dual functionality might enhance the oxygen reduction performance of FeNi-CA [54]. Pore size distributions were obtained by analyzing the desorption branches of the isotherms using the BJH (Barrett–Joyner–Halenda) method [55]. As shown in Fig. 1 (c), Ni-CA has a saturated adsorption plateau at smaller P/P_0 and features mesopores with sizes centered at 8.6 nm, while FeNi-CA and Fe-CA have a relatively wider pore size distribution with pore diameters centered on ~20 nm and ~25 nm, respectively. The N_2 adsorption–desorption analysis yielded pore structural parameters that are presented in Table 1, with results indicating the single metal Ni-CA has the highest BET surface area and smallest average pore diameter amongst the three cathodes. Nevertheless, both the FeNi-CA and monometallic Fe-CA have similar pore structural parameters, and BET surface areas of around 600 m^2/g which are larger than other reported alloy carbon aerogels [34,41,56]. Such a highly porous characteristic can provide an increased number of catalytically active sites, as well as ample contact area between electrolyte and electrode for efficient electrocatalysis [57].

The surface morphology of FeNi-CA was further examined using high-resolution scanning electron microscopy (HRSEM). The HRSEM images under 25 K magnification (Fig. 2 (a)) show that the synthesized FeNi-CA has a networked porous microstructure. Moreover, aggregated nanoclusters may be observed from the images under higher magnifications (Fig. 2 (b)). According to a previous study [58], the obtained cathode presents as a typical carbon aerogel structure, being comprised

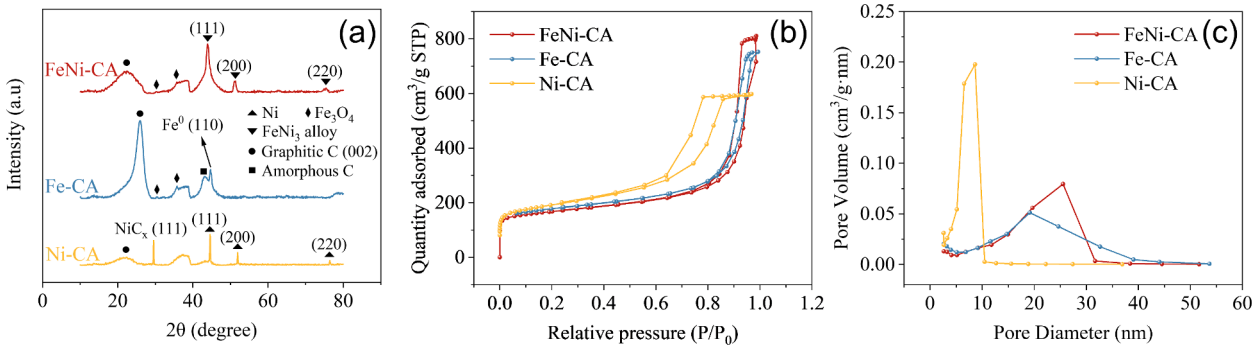

Fig. 1. (a) XRD spectra, (b) N_2 adsorption–desorption isotherms, and (c) Pore size distribution curves of FeNi-CA, Fe-CA, and Ni-CA.

Table 1
Metal loading and porosity of FeNi-CA, Fe-CA, and Ni-CA.

Electrode	Metal loading [wt.%]		BET surface area (m^2/g)	Micropore area (m^2/g)	Micropore volume (cm^3/g)
	Fe	Ni			
FeNi-CA	1.15 ± 0.01	0.86 ± 0.02	589.0	350.9	0.155
Fe-CA	1.05 ± 0.04	/	609.7	351.0	0.162
Ni-CA	/	0.90 ± 0.05	665.9	301.2	0.138

of rounded and interconnected primary clusters.

The microstructure of FeNi-CA was then characterized using high-resolution transmission electron microscopy (HRTEM) and scanning transmission electron microscopy (STEM). The STEM images in Fig. 2 (c) indicate nano-scale particles with a size range of 10–20 nm that are well dispersed within the carbon aerogel matrix, ensuring that they maintained high dispersion during the preparation process. Elemental C, Fe and Ni are clearly evidenced by the energy dispersive X-ray spectroscopy (EDS) mappings in Fig. 2 (d) and (e), as well as further images supplied in the Electronic Supplementary Materials (ESM, Fig. S3 (a)–(d)). The distribution of these elements reveals that Fe signals match Ni signals, indicating the formation of an alloy phase in the carbon aerogel structure, which is further demonstrated by the electron diffraction ring corresponding to $FeNi_3$ (1 1 1) plane with an interplanar spacing of 0.204 nm in Fig. 3 (a). The presence of certain transition metals (e.g., Fe, Ni, Cr) has been reported to catalyze the formation of graphite clusters during the carbonization stage of carbon aerogel [59,60]. A detailed examination of Fig. 3 (b) shows partial graphitization of the carbon phase around the alloy particles. Furthermore, the interplanar spacing of 0.253 nm depicted in Fig. 3 (c) confirms the presence of Fe_3O_4 within the FeNi-CA composite, which is consistent with the findings obtained from XRD analyses. Additionally, the measured interplanar spacing of 0.341 nm can be attributed to the (0 0 2) crystal plane of graphitic carbon [61]. Previous research [59] has also observed partial graphitization of the carbon aerogel. The formation of these graphitic clusters is likely to enhance the electrochemical performance of the materials by increasing their electrical conductivity [55].

In addition to the alloy particles, there are also free metals found in the carbon matrix that may be associated with bound ions. The atomic percentage of Fe and Ni in the selected area of Fig. S3 (a) (including free and alloy phases) is 43.7 % (Fe) and 56.3 % (Ni), as confirmed by the EDS spectrum (Fig. S3 (e)), almost in accordance with the input molar ratio during synthesis (Fe:Ni = 1:1). Furthermore, the metal loadings determined by inductively coupled plasma-mass spectrometry (ICP-MS) analysis is 1.15 wt% (Fe) and 0.86 wt% (Ni), as shown in Table 1.

Fig. 3 (d)–(f) present STEM images and element mapping taken from

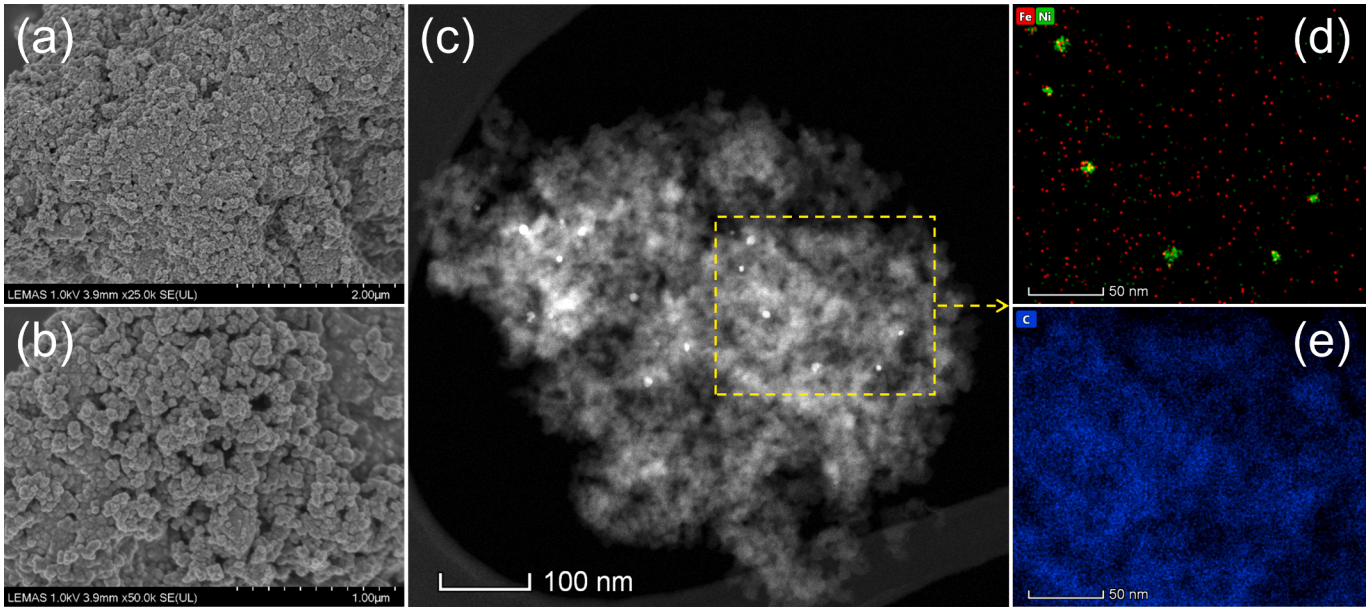

Fig. 2. (a) and (b) HRSEM images of FeNi-CA, (c) STEM image of a FeNi-CA cluster, (d) EDS mapping of elemental Fe and Ni, and (e) EDS mapping of elemental C.

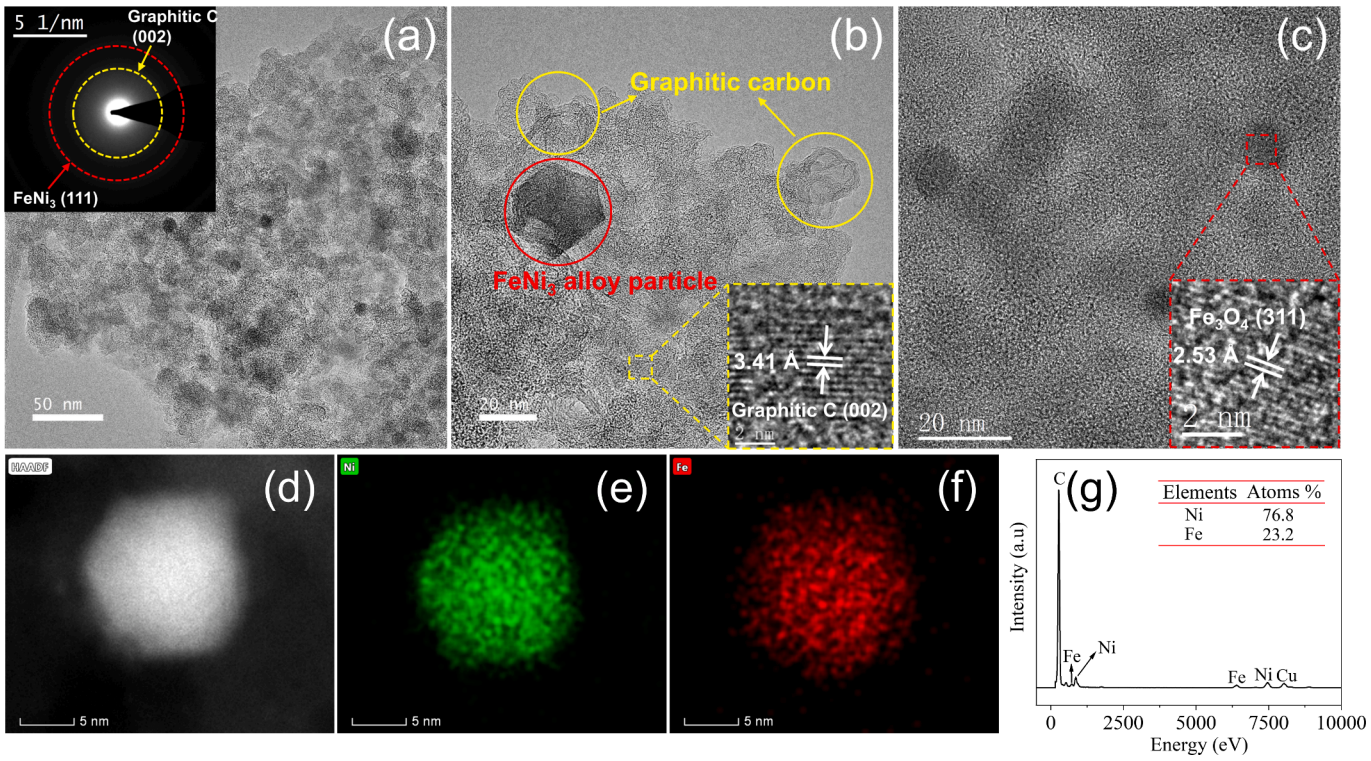

Fig. 3. (a)–(c) HRTEM images of FeNi-CA, (d) STEM image of an individual $FeNi_3$ particle, (e) EDS mapping of elemental Ni, (f) EDS mapping of elemental Fe, (g) EDS spectra of the selected $FeNi_3$ particle.

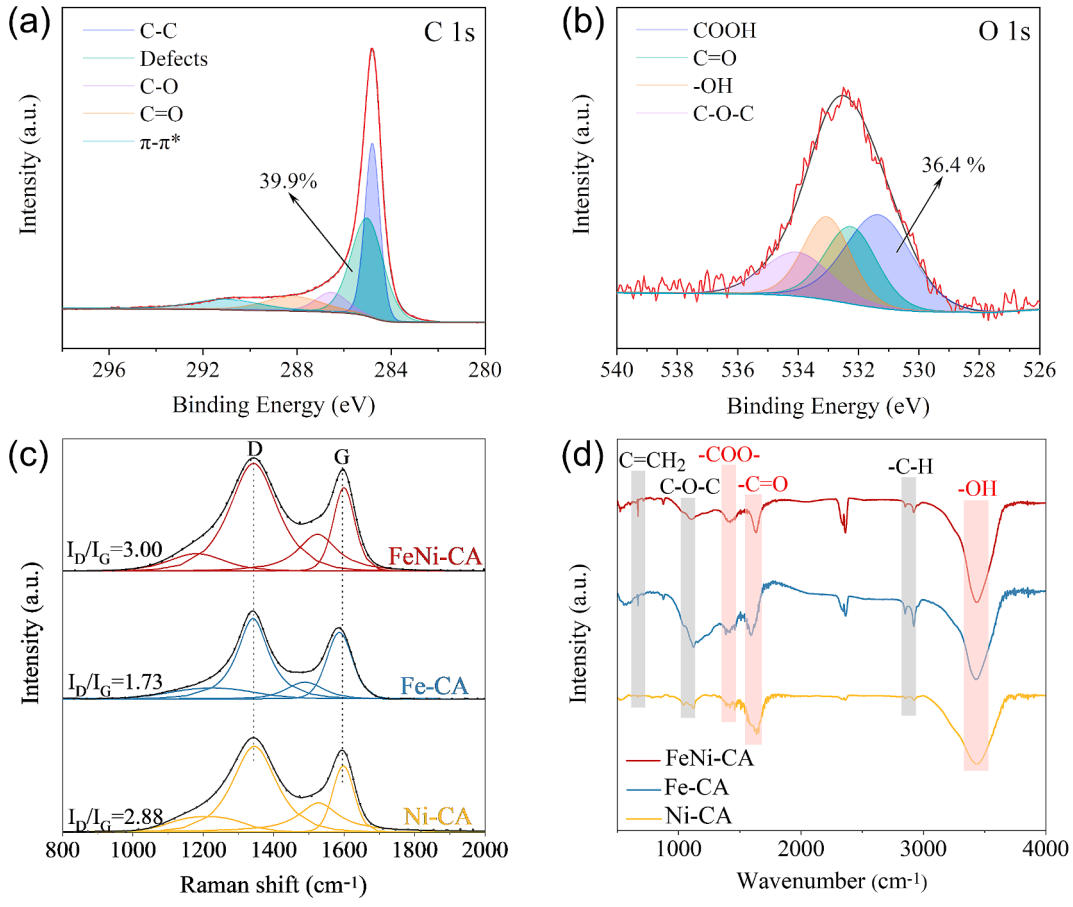

Fig. 4. (a) C 1s XPS spectra of FeNi-CA, (b) O 1s XPS spectra of FeNi-CA, (c) Raman spectra, and (d) FTIR spectra.

an individual alloy particle. These reveal that both elemental Fe and Ni distribute homogeneously in the $FeNi_3$ alloy phase. The line scanning profiles within the ESM (Fig. S4 (a)–(c) and Fig. S5) that were recorded from the alloy particles further confirm the uniform distribution of Fe and Ni. The molar ratio in the alloy particle was measured as 23.2 % (Fe) and 76.8 % (Ni) by the EDS spectrum (Fig. 3 (g)), almost consistent with the stoichiometric ratio in $FeNi_3$ alloy [47]. Previous research also found a $FeNi_3$ alloy phase in a metal–organic framework (MOF) derived three-dimensional carbonaceous matrix. The synergistic effect between Ni and Fe components was shown to play an important role in the electrocatalysis process[62].

X-ray photoelectron spectroscopy (XPS) analysis was performed to investigate the electrode surface, providing insights into the elemental composition and surface functional groups of FeNi-CA. Results for the full spectrum, as well as Fe and Ni peaks, are presented in the ESM (Fig. S6 (a)–(c)) and identify the presence of C and O on the cathode surface within the detection limit. Due to the low metal loadings in the synthesized cathode, the high-resolution XPS spectra of the metal elements exhibit only weak signals. The C 1s XPS spectrum (Fig. 4 (a)) displays distinct peaks representing different carbon species. The peaks at 284.8 eV, 285.0 eV, 286.5 eV, 288.1 eV, and 291.0 eV are assigned to C–C, C defect, C-O, COOH, and π-π*, respectively [50,63]. The presence of carbon defects has been demonstrated to effectively adjust the electronic structure of the catalyst, leading to superior electrocatalytic properties [64]. Raman spectroscopy was subsequently employed to investigate the presence of carbon defects in the synthesized cathodes. As presented in Fig. 4 (c), all samples display characteristic D and G bands at 1350 cm^{-1} and 1590 cm^{-1}, respectively, corresponding to the disordered and graphitic phases in carbon [65]. Hence, the integrated intensity ratio of the D and G bands area indicates the degree of structural ordering and defects in the carbon framework, with a higher I_D/I_G value suggesting increased defects in disordered carbon [64]. The I_D/I_G value is approximately 3.00, 1.73, and 2.88 for the FeNi-CA, Fe-CA, and Ni-CA, respectively. These demonstrate that the incorporation of FeNi nanoalloy promotes the formation of carbon defects, aligning with the results of numerous carbon defects (39.9 % of relative abundance) presented by the C 1 s XPS spectrum.

According to a previous study [66], introduced oxygen functional groups (such as surface –COOH) have a positive impact on the increased efficiency of H_2O_2 generation. This is because of their role in facilitating the displacement of electron density of the active site thereby enhancing interaction during O_2 adsorption [19,67]. The O 1s XPS spectra of FeNi-CA (Fig. 4 (b)) could be deconvoluted into four peaks associated with different oxygen groups, namely –COOH at 531.3 eV, C═O at 532.2 eV, C-O-C at 534.0 eV, and –OH at 533.0 eV [68]. Notably, the FeNi-CA exhibits a high –COOH content and the relative abundance is calculated to be 36.4 %. Fourier transform infrared spectrometer (FTIR) analysis was also conducted to investigate functional groups and chemical bonds. The peaks observed at 3433 cm^{-1} (Fig. 4 (d)) may be attributed to O–H groups, stretching vibrations of –C═O bonds are observed at 1629 cm^{-1}, and peaks at 1419 cm^{-1} are assigned to –COO- vibrations [69]. FTIR analysis also reveals the presence of oxygen functional groups specifically –COOH on the FeNi-CA surface, which has the potential to enhance electrocatalytic ORR reactivity [28].

The combined characteristic analysis showed that FeNi-CA possesses an interconnected carbon network with a prominent mesoporous structure and high surface area. Mesopores function as pathways for gas transfer, delivering oxygen and facilitating the permeation of electrolyte into the interior of carbon materials. The nanostructured morphology of the material provides a larger number of active sites on the electrode surface, promoting enhanced catalytic activity. Additionally, the presence of $FeNi_3$ alloy, carbon defects, and abundant oxygen functional groups further enhance its structural characteristics. These unique structural features endow FeNi-CA alloys as promising candidates for electrocatalytic applications.

3.2. Electrochemical properties

Electrochemical testing is an efficient approach to evaluate the performance of cathodic material samples for an electro-Fenton system. To investigate the conductivity of the synthesized materials, electrochemical impedance spectroscopy (EIS) was conducted and the impedance Nyquist diagram is presented in Fig. 5 (a). A semi-arc in the high-frequency range was observed, representing the charge transfer resistance (R_{ct}) at the interface between the electrolyte and electrode. A larger semi-arc radius represented a greater R_{ct} [70], and the linear response in the low-frequency region corresponded to Warburg impedance reflecting ion diffusion behavior [71]. Both Ni-CA and FeNi-CA showed smaller R_{ct} than Fe-CA, suggesting faster electron transfer rates and higher kinetics for electrochemical reactions [72]. The increased electron transfer efficiency might be due to the chemical interactions such as the electron exchange at the interface of FeNi alloy particles and the carbon matrix [41]. Cyclic voltammetry (CV) experiments were carried out to evaluate the electrocatalytic activity of the FeNi-CA cathode. No redox peaks were detected in the electrolyte saturated with N_2 when employing FeNi-CA as the working electrode (Fig. 5 (b)). In comparison, a distinct oxygen reduction peak emerged at −0.5 V vs. reversible hydrogen electrode (RHE), accompanied by an increase in current response. This observation suggested the occurrence of an oxygen reduction reaction (ORR) on the surface of the electrode [73].

In addition, $2e^-$ ORR activity and selectivity of the FeNi-CA, Fe-CA, and Ni-CA electrodes were investigated using rotating ring-disk electrode (RRDE) measurements. Fig. 5 (c) illustrates the measurement of current resulting from oxygen reduction on the disk electrode and the quantification of generated H_2O_2 oxidation currents at 1.3 V vs. RHE on the ring electrode. The onset potential (E_{onset}) for FeNi-CA, Fe-CA, and Ni-CA were determined to be 0.421 V, 0.442 V, and 0.866 V vs. RHE, respectively. Although Ni-CA exhibited the highest ORR activity, as demonstrated by the most positive onset potential, its $2e^-$ ORR selectivity was not as high as FeNi-CA as evidenced by the smaller ring current density. The H_2O_2 selectivity and electron transfer number were calculated according to Eq. S1 and Eq. S2 in the ESM. In the −0.4 to 0.2 V vs. RHE range (Fig. 5 (d)), the H_2O_2 selectivity of the FeNi-CA catalyst was 60 %–80 %, higher than that of the monometallic Fe-CA and Ni-CA. The electron transfer number of FeNi-CA was 2.5–2.7, indicating its activity for catalyzing two-electron ORR processes from oxygen to H_2O_2. The electron transfer number results also showed the Fe-CA electrode had high activity for the $4e^-$ ORR, leading to the formation of H_2O ($O_2 + 4e^- + 4H^+ \rightarrow H_2O$). Therefore, the incorporation of Ni increases the ORR activity and induces the conversion of $4e^-$ oxygen reduction to $2e^-$ pathways. Moreover, the synergistic effect of Fe and Ni greatly enhanced 2e ORR selectivity of pure CA (Fig. S7 (a)-(b)), which contributes to the improved production of H_2O_2 by over four times during the electrocatalytic reaction (Fig. S7 (c)).

The enhanced ORR activity observed in FeNi-CA compared to the monometallic may be primarily attributed to the alloying effect between Fe and Ni that caused lattice mismatch and electronic modification. This alloying effect has been demonstrated in other bimetallic alloys and is known to enhance catalytic performance [74]. The increased ORR activity of FeNi-CA could therefore be ascribed to (1) the presence of transition metals catalyzing the partial graphitization of the carbon aerogel to increase electrical conductivity, and the graphitic carbon further promoting the development of carbon defects. Here, the carbon defects could modify the atomic and electronic structure of the cathode, resulting in significantly improved electrocatalytic properties [26]; (2) the unique graphitic carbon structure contributed to the generation of oxygen functional groups, which played a beneficial role in enhancing the ORR electrocatalytic process; and (3) the formation of FeNi alloy facilitated efficient electron transport within the electrode, improving overall electrochemical performance [75].

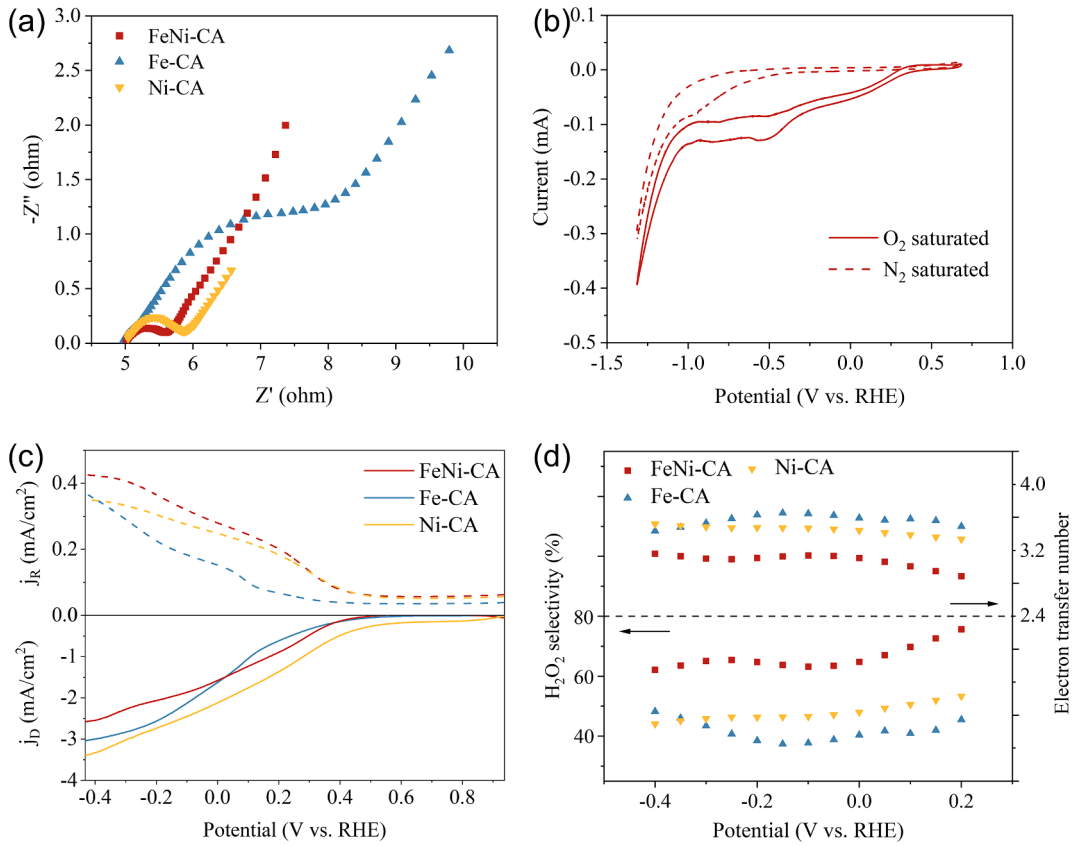

Fig. 5. (a) EIS Nyquist plots, (b) CV curves of FeNi-CA in the presence O_2 and N_2, (c) Polarization curves of different electrodes and simultaneous H_2O_2 oxidation currents at the ring electrode in 0.1 mol/L Na_2SO_4 at pH = 3, and (d) Calculated electron transfer number and H_2O_2 selectivity.

3.3. Electro-Fenton oxidation performance

3.3.1. Degradation efficiency of ACT

In Section 3.2, the FeNi-CA cathode exhibited high $2e^-$ ORR activity and selectivity, providing essential conditions for the heterogeneous electro-Fenton (EF) reaction. The electro-Fenton performances of synthesized cathodes were investigated using acetaminophen (ACT), a common analgesic agent, as the model pollutant under an initial pH of 7. Data for EF and electro-sorption (ES) degradation of ACT with the alloy and monometallic catalysts are presented in Fig. 6 (a), along with that for the commercial graphite sheet cathode. The degradation of ACT in electro-Fenton systems followed Pseudo-first-order kinetics, as evidenced by the high linear correlation coefficients (R^2 values) (see Fig. S8 (a)). The degradation of ACT using a graphite sheet as the cathode reached 43 % after 2 h (Fig. 6 (a)) with an apparent rate constant (k_{obs}) of 0.005 min^{-1} (see Fig. S8 (b)). In comparison, the ACT degradation improved with the Fe-CA and Ni-CA electrodes (both to ~45–50 %), with corresponding increases in the k_{obs}, reaching 0.009 and 0.006 min^{-1}, respectively.

The electro-sorption performance was assessed at an operational current of 1 mA and 0.2 L/min N_2 atmosphere. The results showed the FeNi-CA, featuring a porous structure and high surface area, achieved 53 % electrochemical sorption capacity for ACT. In comparison to the monometallic cathodes, ACT degradation with FeNi-CA in the EF system

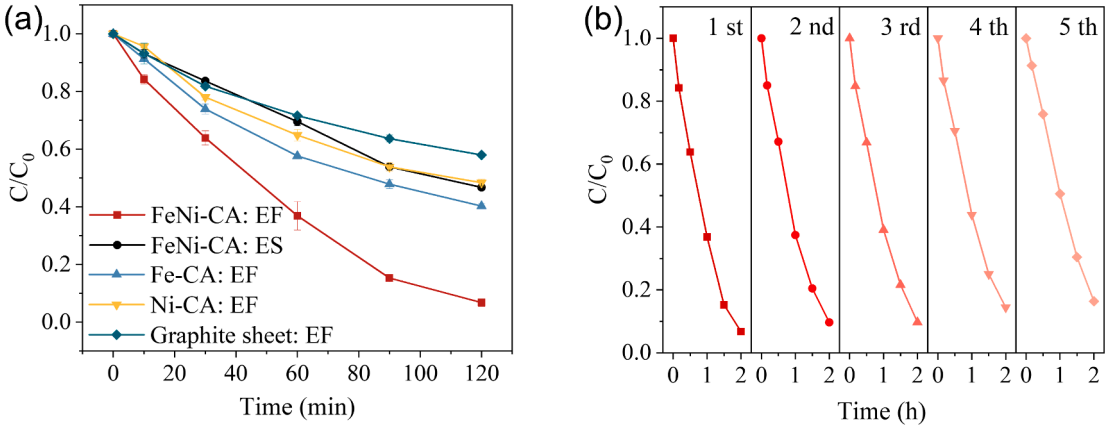

Fig. 6. (a) ACT degradation in electro-Fenton (EF) and electro-sorption (ES) system, (b) Recycle use performance of FeNi-CA cathode in EF system. Conditions: ACT-10 mg/L, Na_2SO_4-50 mM, pH_0-7.0, 0.4 L/min compressed air and 20 mA for EF system, 0.2 L/min N_2 and 1 mA for ES system.

significantly increased to 93 % within 120 min. The rate constant improved from 0.006 min^{-1} to 0.021 min^{-1} indicating enhanced reactivity of catalytic oxidative degradation. Furthermore, the electrical energy consumptions (EC) and electricity costs for FeNi-CA, Fe-CA, and Ni-CA based EF processes were evaluated according to Eq. (4), the calculation results are shown in Table 2. The average business electricity unit rate for the UK is 27p/kWh in 2024 [76].The calculation results indicate that FeNi-CA based EF system has the highest electrocatalytic performance in ACT degradation with the lowest energy consumption compared to Fe-CA and Ni-CA. Moreover, a positive synergistic effect (SE) value according to Eq. (5) indicates that the sole metals Fe and Ni have a beneficial synergistic effect on improving the electrocatalytic activity. The electrochemical performances of FeNi-CA cathodes with different metal content ($Fe_{0.5}Ni_{0.5}$-CA, $Fe_{0.7}Ni_{0.3}$-CA, and $Fe_{0.3}Ni_{0.7}$-CA) were also compared in Fig. S9. The results show that $Fe_{0.5}Ni_{0.5}$-CA with Fe: Ni molar ratio of 1:1 exhibited the highest efficiency on ACT degradation.

The reusability of FeNi-CA was further studied under otherwise identical conditions by reusing the washed and dried cathode in subsequent runs. In this case, ACT degradation in the electro-Fenton system with FeNi-CA still reached 84 % over five consecutive runs after 120 min (Fig. 6 (b)), demonstrating relatively high stability and reusability of the cathode. It is noted that the degradation continues after the set time period and would still lead to more organic breakdown, with a slightly reduced reaction rate constant (Fig. S10 (a)–(b)). The above findings demonstrated that the incorporation of Fe and Ni with molar ratio of 1:1 on the carbon aerogel nanostructure effectively improved the performance of contaminant degradation. Here, the removal of ACT in the FeNi-CA electro-Fenton system was induced by the simultaneous effects of oxidation degradation and electro-sorption.

In general, the degradation of organic contaminants involves both direct and indirect oxidation processes. Indirect oxidation is usually triggered by the production of reactive free radicals [77]. To further investigate the role of free radicals in ACT degradation with the FeNi-CA cathode, quenching experiments were conducted using *tert*-butanol (TBA) as an $^{\bullet}OH$ scavenger and p-benzoquinone (p-BQ) as a $^{\bullet}O_2^-$ scavenger [25,29], as given in Fig. 7 (a) (corresponding degradation data and Pseudo-first-order fit are given within the ESM, Fig. S11). Indeed, the k_{obs} of ACT removal decreased from 0.021 min^{-1} to 0.006 min^{-1} when TBA was added to the system, indicating that ACT was eliminated through catalytic oxidation by $^{\bullet}OH$. Additionally, about half the apparent rate constant drop was observed in the presence of p-BQ, indicating the presence of $^{\bullet}O_2^-$. These findings suggest that O_2 undergoes an initial reduction to $^{\bullet}O_2^-$ *via* a 1-electron pathway ($O_2 + e^- \rightarrow \bullet O_2^-$) [41], followed by subsequent reduction to H_2O_2 and conversion to $^{\bullet}OH$. It was noted that ACT was still partially degraded even after the capture of $^{\bullet}OH$, which may be attributed to the effect of electro-sorption processes.

The generation of $^{\bullet}OH$ and $^{\bullet}O_2^-$ species was further verified by electron spin resonance (ESR) spectroscopy using DMPO as the spin-trapping agent, as shown in Fig. 7 (b). The four-line characteristic signal with a relative intensity of 1:2:2:1 was detected as the typical spectrum of DMPO-OH spin adducts, confirming the presence of $^{\bullet}OH$ radical in the FeNi-CA EF process [78]. Additionally, the sextuplet ESR spectrum for DMPO-O_2 spin adducts proved the production of $^{\bullet}O_2^-$ species during the reaction [79]. Overall, these results indicated that the ACT degradation in the FeNi-CA electro-Fenton system was dominated by indirect oxidation mechanisms with $^{\bullet}OH$ radicals playing a primary role. The generation of $^{\bullet}OH$ was also directly proved by its probe reaction product with 0.01 M salicylic acid [80], which showed that 112 μmol/L of $^{\bullet}OH$ was finally produced after 120 min reaction in the EF system using FeNi-CA as the cathode (dash blue line in Fig. 7 (c)).

Interestingly, the level of electro-generated H_2O_2 using FeNi-CA was quantified and found to be relatively low, measuring around 38.8 ± 0.64 μmol/L (solid red line in Fig. 7 (c)) after 2 h. The low concentration of H_2O_2 observed with FeNi-CA, despite its high activity and selectivity for the $2e^-$ ORR, is likely due to it undergoing rapid on-site decomposition as an intermediate to produce reactive $^{\bullet}OH$ [34]. According to other studies [81], the presence of encapsulated alloy nanoparticles in carbon materials allowed for the modulation of the local electronic environment, which in turn activated H_2O_2 through a $1e^-$ pathway, leading to the generation of $^{\bullet}OH$. Besides, the presence of Fe_3O_4 on the surface is capable of catalyzing the activation of H_2O_2 to $^{\bullet}OH$. To explore the mechanism of H_2O_2 reduction to $^{\bullet}OH$ with FeNi-CA, ACT degradation efficiency and $^{\bullet}OH$ generation in the system containing 0.1 g/L FeNi-CA powder and 50 ppm externally supplied H_2O_2 were measured. As depicted in Fig. S12, 69 % of ACT removal and 89.9 μmol/L of $^{\bullet}OH$ production were observed after 2 h reaction. Therefore, it could be concluded that FeNi-CA functioned not only as an efficient cathode inducing $2e^-$ ORR but also as a heterogeneous Fenton-like catalyst for the activation of H_2O_2 to produce $^{\bullet}OH$ radicals.

Table 2
Energy consumption for three EF systems. Operational conditions: ACT-10 mg/L, Na_2SO_4-50 mM, pH_0-7.0.

EF system	I (A)	V (V)	t (h)	Δm_{ACT} (g)	EC_{ACT} (kWh/kg_{ACT})	Electricity cost (£/kg_{ACT})
FeNi-CA	0.02	2.455	2	1.2375×10^{-3}	79.35	21.42
Fe-CA	0.02	2.62	2	0.825×10^{-3}	127.03	34.30
Ni-CA	0.02	2.515	2	0.705×10^{-3}	142.70	38.53

3.3.2. Optimization of key parameters

Optimizing reaction parameters was beneficial in further enhancing degradation performance, as shown in Fig. 8. The influence of air flow rate on ACT degradation efficiency was investigated, and found to be insignificant (Fig. 8 (a)). The k_{obs} at flow rates of 0, 0.2, 0.4, and 0.6 L/min were found to be 0.015, 0.016, 0.020, and 0.015 min^{-1} (inset), respectively. These findings suggested that ACT could be efficiently removed even in the absence of external aeration, achieving ~84 % removal after 2 h. The dissolved oxygen (DO) concentration under different air flow rates before and after the reaction was also measured using a digital multi-meter kit with a luminescent dissolved oxygen probe, and the results are shown in Fig. 8 (b). The DO concentration in the zero-aeration system reached 16.5 mg/L after the reaction, accompanied by a change in pH from 7 to 3. The possibility of pH reduction caused by intermediate products of ACT degradation (such as organic acids) has been experimentally ruled out in Fig. S13, which shows that the pH dropped from 7 to about 3 in the absence of any contaminants. Besides, small bubbles were also observed around the anode during the reaction. It can be speculated that in the zero-aeration system, an oxygen evolution reaction (OER) occurred at the platinum anode, resulting in an increase in dissolved oxygen concentration and a decrease in pH (Eq. (6) [14,82]. Similar mechanisms of oxygen generation from OER anode without aeration have been also reported in other electrochemical systems [83–85]. The above results indicated that the oxygen generated from the anodic reaction was effectively utilized by the FeNi-CA cathode for the formation of H_2O_2. As discussed earlier, the FeNi-CA cathode had a large surface area and large pore volume, enabling enhanced adsorption, storage, and mass transfer of dissolved O_2 for electro-generation of H_2O_2 [86]. Consequently, the O_2 generated at the anode was sufficient to sustain H_2O_2 production even without external aeration, which is a more cost-effective solution compared to previously reported electrochemical H_2O_2 generation under aeration [40,87].

$$2H_2O \rightarrow 4e^- + 4H^+ + O_2 \quad E^0 = 1.23V \tag{6}$$

The impact of current on degradation performance was also examined due to its ability to regulate electron transfer. The degradation rate

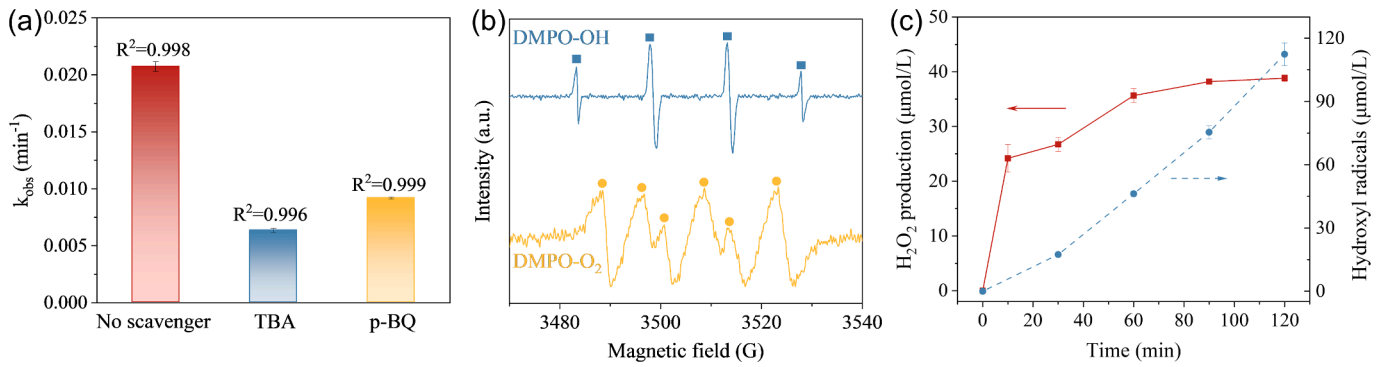

Fig. 7. (a) The effect of radical scavengers on apparent rate constant in FeNi-CA EF system, (b) ESR spectra in FeNi-CA EF system, and (c) H_2O_2 production (red line) and hydroxyl radical generation (blue line) in FeNi-CA EF system. Conditions: ACT-10 mg/L, Na_2SO_4-50 mM, pH_0-7.0, 20 mA, without aeration, TBA-1 M, p-BQ-2 mM. (For interpretation of the references to colour in this figure legend, the reader is referred to the web version of this article.)

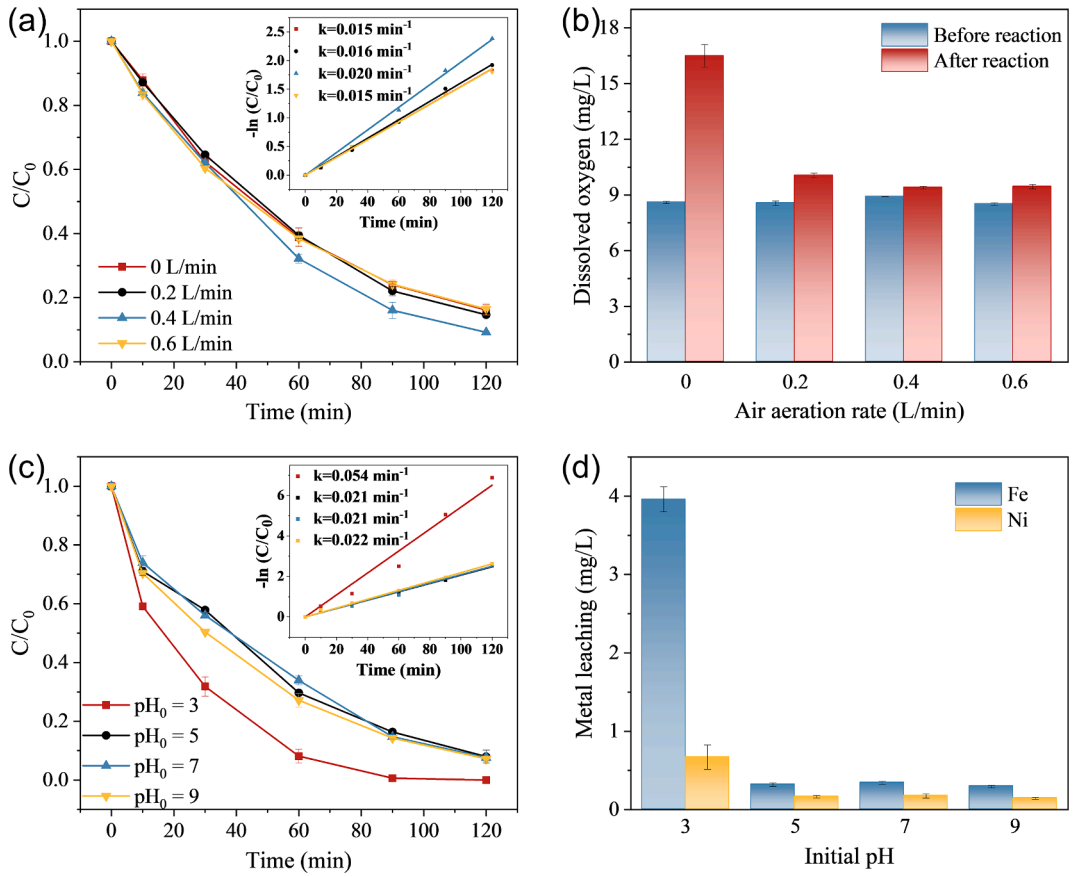

Fig. 8. (a) The effect of air aeration rate on ACT degradation, (b) Dissolved oxygen concentrations before and after reaction under different air aeration rates, (c) The effect of initial pH on ACT degradation, and (d) Metals leaching after 120 min under different initial pH Conditions: ACT- 10 mg/L, Na_2SO_4-50 mM.

of ACT varied with current, and reaction efficiency increased to an extent with current ranging from 10 mA to 20 mA (Fig. S14). The electron transfer rate increased with the current values, which may be advantageous for the generation of H_2O_2 and consequent production of a greater quantity of reactive radicals [88]. However, final ACT degradation at 10 mA was slightly higher than that of 20 mA, and a decrease in ACT removal efficiency was observed at higher current conditions such as 30 mA and 40 mA. In these cases, k_{obs} decreased from 0.02 min^{-1} to 0.013 min^{-1} when the current was increased from 20 mA to 40 mA. This may be attributed to a higher four-electron reduction of oxygen reaction rate (Eq. (7) [89], and the occurrence of a side reaction involving hydrogen evolution ($2H^+ + 2e^- \rightarrow H_2$) [90]. These factors are unfavorable for H_2O_2 generation, leading to a decrease in the efficiency of ACT degradation. The highest degradation efficiency of ACT was achieved at a current of 10 mA (current density of 2.2 mA/cm^2), resulting in ACT removal of 94 % within 120 min at an initial pH of 5.8.

$$O_2 + 2H_2O + 4e^- \rightarrow 4OH^- E^0 = 1.23Vvs.RHE \quad (7)$$

In addition to the aeration rate and current, the effect of initial pH on oxidation performance in the FeNi-CA EF process was also investigated. These results demonstrated that increasing initial pH from 3.0 to 9.0 led to a slight decrease in degradation efficiency from 99.9 % to 92.8 % after 120 min, along with a drop in the rate constant from 0.054 min^{-1} to 0.022 min^{-1} (Fig. 8 (c)). Considering pH is known to be a critical factor

affecting metal leaching [91], the concentrations of dissolved metal ions under different initial pH conditions were also examined in Fig. 8 (d). Although the system at initial pH 3 exhibited the highest oxidation ability, it resulted in a release of Fe ions, as measured post-reaction. It is likely the major source of the leached metals was free metals (as observed in Fig. 2) rather than the alloy nanoparticles, because the carbon aerogel can provide a porous matrix that physically encapsulates the FeNi nanoparticles, thus stabilizing them and reducing leaching [41,50].

Considering the leaching metals, the contribution of the homogeneous Fenton reaction (Eq. (2) in ACT decomposition at an initial pH of 3 was further illustrated in Fig. S15. The results show that although the homogeneous Fenton process appeared to have much slower kinetics possibly due to limitations in radical generation, the leached metal ions, acting as homogeneous Fenton catalysts, contributed to over 30 % of the ACT degradation at an initial pH of 3. Furthermore, a desirable degradation rate (over 90 % after 120 min) was still achieved at higher initial pH (5, 7, and 9) with controlled metal leaching levels (Fig. S16), thus indicating the potential of the established EF system in practical applications. It should also be noted that metal leaching significantly decreased after pretreating the FeNi-CA cathode in the absence of any contaminant (Fig. S17), effectively controlling any secondary pollution caused by released metal ions.

The variation of pH values before and after the reaction was also recorded (Fig. S18). This data indicated that under all pre-reaction conditions, the pH decreased to around 3 after the degradation process where OER at the anode led to the generation of H^+ (Eq. (6). Conversely, the formation of H_2O_2 through the $2e^-$ reduction (Eq. (1) and $1e^-$ reduction pathways for $^{\bullet}OH$ radicals ($H_2O_2 + e^- \rightarrow \bullet OH + OH^-$) required the involvement of H^+. Thus, the anodic oxygen evolution could be regarded as an induction stage that provided oxygen source and favorable acid condition to subsequent oxygen reduction and Fenton-like reactions.

3.4. Degradation mechanisms, pathways, and comparison of other EF technologies

The synergistic effect observed in the FeNi-CA system can be attributed to three key interactions and enhancements brought about by the co-presence of Fe and Ni: (1) Structural enhancement. FeNi-CA exhibits a high surface area and prominent mesoporous structure. Such a highly porous characteristic can provide more active catalytic sites, which allows for more effective interactions with the target pollutants and leads to enhanced degradation rates. Besides, mesopores serve as conduits for gas transfer, enabling the delivery of oxygen and enhancing the infiltration of electrolyte into the inner structure of carbon materials. (2) Improved electrocatalytic properties. The formation of the FeNi alloy enhances electron transport within the electrode, while the presence of transition metals catalyzes the partial graphitization of the carbon aerogel, thereby increasing its overall electrical conductivity. Additionally, the incorporation of the FeNi nanoalloy encourages the development of carbon defects. These defects play a crucial role in modifying the electronic structure of the catalyst, which in turn significantly improves its electrocatalytic properties. (3) Increased ORR activity and selectivity. The unique graphitic carbon structure facilitates the formation of oxygen functional groups, which play a beneficial role in enhancing the ORR electrocatalytic process. Additionally, the alloying of Fe and Ni leads to lattice mismatches and electronic modifications, which further improve the activity and selectivity of the ORR.

The degradation mechanism of ACT in the electro-Fenton oxidation system with FeNi-CA may be summarized as follows (Fig. 9): an initial current-induced oxygen evolution reaction occurs at the platinum anode, resulting in increased concentrations of dissolved oxygen and H^+ ions in the electrolyte. The generated oxygen diffuses into the cathode/electrolyte interface where it is utilized in the electro-generation of H_2O_2. The unique microstructure of the FeNi-CA cathode enables high oxygen utilization efficiency, thus eliminating the need for external aeration. Additionally, the OER generates H^+ ions to create a favorable pH for the two-electron ORR and subsequent activation of H_2O_2. The

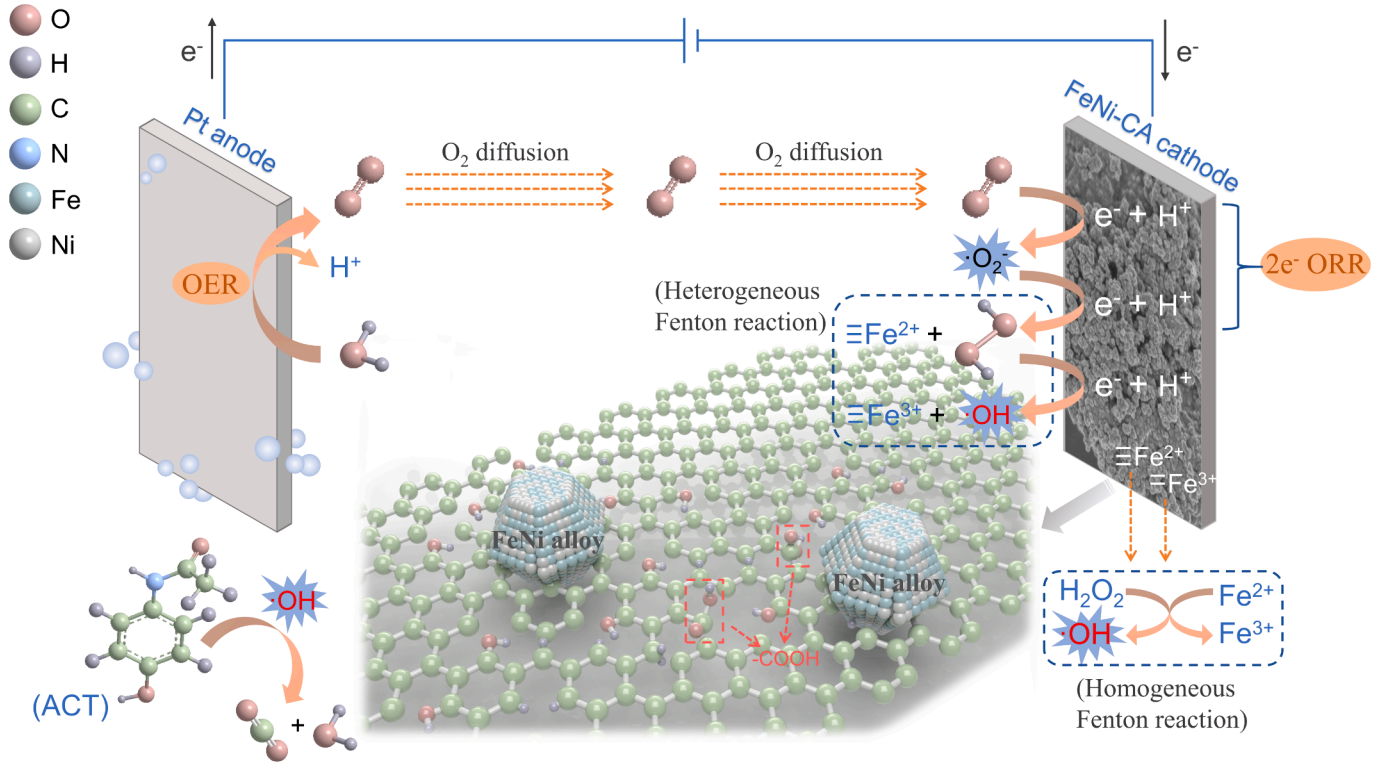

Fig. 9. Mechanisms of radical generation and ACT degradation in FeNi-CA EF system.

diffused oxygen then undergoes an initial $1e^-$ reduction pathway, forming intermediate $^{\bullet}O_2^-$ that is then further reduced to produce H_2O_2. Subsequently, H_2O_2 undergoes conversion to $^{\bullet}OH$ radicals through a heterogeneous Fenton reaction (Eq. (8) [81] catalyzed by multi-valence iron on surface Fe_3O_4, and a homogeneous Fenton reaction (Eq. (2) mainly catalyzed by iron dissolution under acidic conditions. Finally, the target compound ACT is efficiently removed through a combination of electro-sorption processes and oxidative reactions dominated by the highly reactive $^{\bullet}OH$ radicals.

The proposed system exhibited three distinctive characteristics: (1) the OER at the anode created favorable pH conditions for the oxygen reduction reaction and H_2O_2 activation at the cathode. (2) Generated oxygen via OER and the high oxygen utilization activity of FeNi-CA eliminated the need for external aeration. (3) The synergistic effect of Fe and Ni components endowed the FeNi-CA cathode with unique structural characteristics including alloy nanoparticles, carbon defects, and abundant oxygen functional groups, thus achieving the dual functionality of $2e^-$ ORR and H_2O_2 activation.

$$\equiv Fe(II) + H_2O_2 + H^+ \rightarrow \equiv Fe(III) + \bullet OH + H_2O \quad (8)$$

The main degradation intermediates of ACT in the FeNi-CA electro-Fenton system were identified using LCMS (Fig. S19) and listed in Table S1. Based on the detected intermediates, and referring to ACT degradation processes reported in other studies, a possible oxidation pathway of ACT by $^{\bullet}OH$ radicals has been proposed (Fig. 10). ACT oxidation begins with $^{\bullet}OH$ attack on the acetyl-amino group and simultaneous hydroxylation (Route I), leading to the formation of N-(3,4-dihydroxyphenyl) formamide (P1) [92]. The detected N-(3,4-dihydroxyphenyl) acetamide (P2) and N-(2,4-dihydroxyphenyl) (P3) indicate the occurrence of hydroxylation reactions at the o- and m-positions of ACT (Route II) [93–95]. Further oxidation leads to the formation of aromatic intermediates 4-(methylamino) phenol (P4) and benzoic acid (P6), and a ring-opened product (P5) with concomitant generation of acetamide (P7) [96,97]. Subsequently, all aromatic by-products undergo further degradation, resulting in the production of aliphatic organic acids such as succinic acid (P8), 3-hydroxypropanoic acid (P10), and oxalic acid (P11) [95,98]. At the same time, ethanamine (P12) is produced by further attack of the alkyl chain of acetamide (P7) and butan-1-amine (P9) by hydroxyl radicals. At the end of the degradation process, all final by-products undergo a complete transformation to CO_2, H_2O, and inorganic ions [99].

The removal efficiency of ACT in the proposed FeNi-CA electro-Fenton system was also compared to other reported EF and EF-based technologies, as summarized in Table 3. Although some of the EF-based processes listed demonstrate higher rate constants than those achieved in our study, they require additional chemical inputs such as iron catalysts and hydrogen peroxide, external air/oxygen aeration, or supplementary energy sources like solar light. This results in higher chemical and energy costs compared to our proposed FeNi-CA system, which eliminates the necessity for extra Fenton reagents or aeration. Furthermore, high current densities, such as 50 mA/cm^2, lead to increased energy consumption, raising concerns for future industrial-scale applications. The developed FeNi-CA EF system offers significant advantages in terms of reaction rate, cost-effectiveness, and environmental compatibility, positioning it as a promising advanced oxidation process technology for wastewater treatment.

4. Conclusions

This study constructed a hetero-EF system composed of OER and

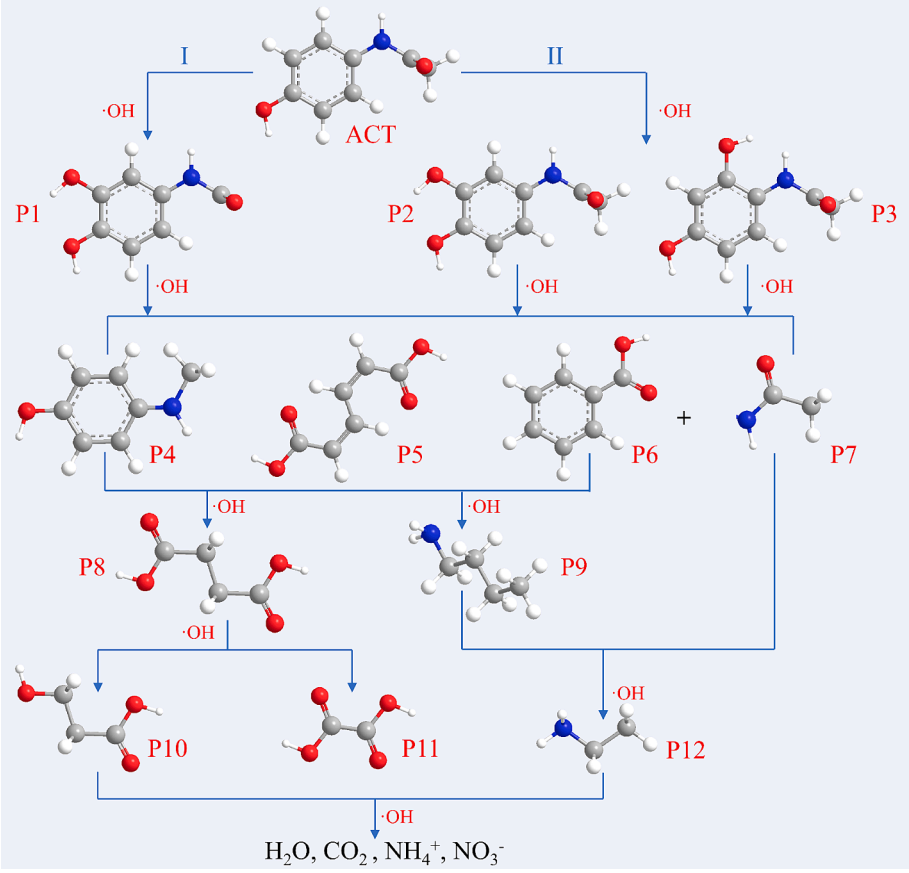

Fig. 10. Proposed degradation pathways of ACT (grey-C atom, red-O atom, white-H atom, blue- N atom). (For interpretation of the references to colour in this figure legend, the reader is referred to the web version of this article.)

Table 3
Comparison with other EF and EF-based technologies for ACT removal.

Study	Electrochemical method	Experimental conditions	Current density (mA/cm^2)	C_{ACT} (mg/L)	ACT removal	k_{obs} (min^{-1})
This work	Electro-Fenton	0.05 M Na_2SO_4 at pH 3	4.44	10	99.4 % within 90 min	0.054
[95]	Dynamic cross-flow electro-Fenton process coupled to anodic oxidation	[Fe^{2+}] = 0.2 mM, with 0.05 M Na_2SO_4 at pH 3 (Cathode: graphite membrane, anode: Ti/Ti_4O_7 rod)	4.42	15.1	/	0.011
[98]	Electro-Fenton	0.05 M Na_2SO_4 at pH 3, aeration rate = 1 L/min (Cathode: carbon-felt, anode: Ti_4O_7 ceramic)	2.5	30.2	95 % within 60 min	/
[100]	HNPs/electro-Fenton	0.01 M Na_2SO_4 at pH 5, hematite nanoparticles (HNPs) = 0.15 g/L (Cathode: carbon felt, anode: platinum sheet)	5.11	20	/	0.030
[101]	CuCoFe-LDH /electro-Fenton	0.05 M Na_2SO_4 at pH 5, CuCoFe-LDH = 0.5 g/L, 0.4 L/min air(Cathode: graphite felt, anode: dimensionally stable anode (DSA) with IrO_2 and RuO_2 coating)	10	20		0.0593
[102]	Goethite/electro-Fenton	At pH 3, goethite = 0.5 g/L (Cathode: carbon-polytetrafluoroethylene, anode: Pt)	12	100		0.0029
[103]	Electro-Fenton	122.5 μL/L H_2O_2 and 100 mg/L KCl at pH 2.75 (Cathode and anode: iron plate)	8	5.75		0.6718
[96]	Electro-Fenton	0.087 mM Fe^{2+} and 16.3 mM H_2O_2 at pH 3 (Cathode: stainless steel, anode: titanium coated RuO_2/IrO_2-coated DSA)	3.8	755	98 % within 120 min	/
[99]	Electro-Fenton	0.2 mM Fe^{2+} and 0.05 M Na_2SO_4 at pH 3, oxygen aeration. (Cathode: carbon felt, counter electrode: platinum cylindrical mesh)	8.3	151	100 % within 240 min	/
[104]	Solar photo electro-Fenton	0.4 mM Fe^{2+}, 0.05 M Na_2SO_4 at pH 3, (Cathode: air-diffusion electrode, anode: Pt sheet)	50	157		0.062

ORR processes using a novel FeNi alloy carbon aerogel as a bifunctional cathode for ACT removal. The FeNi-CA exhibited a typical carbon aerogel structure with a large surface area, nano alloy particles ($FeNi_3$), carbon defects, and oxygen-functional groups, resulting in enhanced 2e$^-$ ORR reactivity and selectivity. Incorporating Fe and Ni components on FeNi-CA endowed it with a fast electron transfer rate, high oxygen utilization efficiency, and superior electrocatalytic properties. In this EF system, FeNi-CA exhibited dual functionality as an efficient cathode enabling 2e$^-$ ORR and as a Fenton-like catalyst for H_2O_2 activation into $^{\bullet}OH$ radicals through proposed heterogeneous and homogeneous pathways. FeNi-CA can achieve efficient removal of ACT across a broad pH range of 3–9 while maintaining good catalytic activity after 5 consecutive cycles. Importantly, this was achieved without the requirement for external aeration, making the process significantly more industrially applicable. Optimization of reaction parameters enabled up to 99.9 % removal of ACT through electro-Fenton oxidation and electro-sorption process after 120 min. Furthermore, ACT degradation intermediates were identified and a reasonable degradation pathway has been proposed. This research has provided valuable insights for the advancement of innovative bifunctional cathodes for electro-Fenton systems with a target of sustainable wastewater treatment. We believe this system to be highly efficient and cost-effective compared to other reported EF processes and, as such, plan further experiments with other candidate pollutants and integration into a continuous flow system.

CRediT authorship contribution statement

Qian Ye: Writing – original draft, Visualization, Investigation, Formal analysis, Conceptualization. **Timothy N. Hunter:** Writing – review & editing, Supervision, Resources, Methodology, Conceptualization. **Hao Xu:** Writing – review & editing, Methodology. **David Harbottle:** Writing – review & editing, Resources. **Girish M. Kale:** Writing – review & editing, Resources. **Martin R. Tillotson:** Writing – review & editing, Supervision, Resources, Methodology, Conceptualization.

Declaration of competing interest

The authors declare that they have no known competing financial interests or personal relationships that could have appeared to influence the work reported in this paper.

Data availability

The data of this study are openly available from the University of Leeds Data Repository at https://doi.org/10.5518/1546.

Acknowledgements

Qian Ye receives funding from the China Scholarship Council (CSC, 202106240065) under the Ministry of Education of P.R. China. The authors express their gratitude to the funding organizations for their support in conducting this research.

The authors extend their appreciation to the individuals at the University of Leeds who have provided technical assistance and training: Dr. Jeanine Williams (HPLC and LCMS), Ms. Karine Alves Thorne (metal loading measurements), and Dr. Ben Douglas (BET). Additionally, we would like to thank Ms. Karen Stevens, Dr. David Elliott, Mr. Morgan McGowan, and Ms. Emma Tidswell for their guidance on the safe setup and operation of the equipment.

Appendix A. Supplementary data

Supplementary data to this article can be found online at https://doi.org/10.1016/j.seppur.2024.128436.

References

[1] L.A. Pérez-Estrada, S. Malato, W. Gernjak, A. Agüera, E.M. Thurman, I. Ferrer, A. R. Fernández-Alba, Photo-fenton degradation of diclofenac: identification of main intermediates and degradation pathway, Environ. Sci. Technol. 39 (2005) 8300–8306, https://doi.org/10.1021/es050794n.

[2] N. Villota, J.I. Lombraña, A. Cruz-Alcalde, M. Marcé, S. Esplugas, Kinetic study of colored species formation during paracetamol removal from water in a semicontinuous ozonation contactor, Sci. Total Environ. 649 (2019) 1434–1442, https://doi.org/10.1016/j.scitotenv.2018.08.417.

[3] W.-C. Yun, K.-Y.-A. Lin, W.-C. Tong, Y.-F. Lin, Y. Du, Enhanced degradation of paracetamol in water using sulfate radical-based advanced oxidation processes catalyzed by 3-dimensional Co3O4 nanoflower, Chem. Eng. J. 373 (2019) 1329–1337, https://doi.org/10.1016/j.cej.2019.05.142.

[4] E.S. Fisher, S.C. Curry, Chapter Ten - Evaluation and treatment of acetaminophen toxicity, in: A. Ramachandran, H. Jaeschke (Eds.), Adv. Pharmacol., Academic Press, 2019, pp. 263–272, https://doi.org/10.1016/bs.apha.2018.12.004.

[5] M. Pacheco-Álvarez, R. Picos Benítez, O.M. Rodríguez-Narváez, E. Brillas, J. M. Peralta-Hernández, A critical review on paracetamol removal from different aqueous matrices by Fenton and Fenton-based processes, and their combined methods, Chemosphere 303 (2022) 134883, https://doi.org/10.1016/j.chemosphere.2022.134883.
[6] B.C. Hodges, E.L. Cates, J.-H. Kim, Challenges and prospects of advanced oxidation water treatment processes using catalytic nanomaterials, Nat. Nanotechnol. 13 (2018) 642–650, https://doi.org/10.1038/s41565-018-0216-x.
[7] C.B. Molina, E. Sanz-Santos, A. Boukhemkhem, J. Bedia, C. Belver, J. J. Rodriguez, Removal of emerging pollutants in aqueous phase by heterogeneous Fenton and photo-Fenton with Fe2O3-TiO2-clay heterostructures, Environ. Sci. Pollut. Res. 27 (2020) 38434–38445, https://doi.org/10.1007/s11356-020-09236-8.
[8] W.H. Glaze, J.-W. Kang, D.H. Chapin, The chemistry of water treatment processes involving ozone, hydrogen peroxide and ultraviolet radiation, Taylor Francis (1987), https://doi.org/10.1080/01919518708552148.
[9] I.A. Katsoyiannis, S. Canonica, U. von Gunten, Efficiency and energy requirements for the transformation of organic micropollutants by ozone, O3/H2O2 and UV/H2O2, Water Res. 45 (2011) 3811–3822, https://doi.org/10.1016/j.watres.2011.04.038.
[10] J.M. Campos-Martin, G. Blanco-Brieva, J.L.G. Fierro, Hydrogen peroxide synthesis: an outlook beyond the anthraquinone process, Angew. Chem. Int. Ed. 45 (2006) 6962–6984, https://doi.org/10.1002/anie.200503779.
[11] J. Xu, X. Zheng, Z. Feng, Z. Lu, Z. Zhang, W. Huang, Y. Li, D. Vuckovic, Y. Li, S. Dai, G. Chen, K. Wang, H. Wang, J.K. Chen, W. Mitch, Y. Cui, Organic wastewater treatment by a single-atom catalyst and electrolytically produced H2O2, Nat. Sustain. 4 (2021) 233–241, https://doi.org/10.1038/s41893-020-00635-w.
[12] D. Guo, Y. Liu, H. Ji, C.-C. Wang, B. Chen, C. Shen, F. Li, Y. Wang, P. Lu, W. Liu, Silicate-enhanced heterogeneous flow-through electro-Fenton system using iron oxides under nanoconfinement, Environ. Sci. Technol. 55 (2021) 4045–4053, https://doi.org/10.1021/acs.est.1c00349.
[13] H. Qi, X. Sun, Z. Sun, Porous graphite felt electrode with catalytic defects for enhanced degradation of pollutants by electro-Fenton process, Chem. Eng. J. 403 (2021) 126270, https://doi.org/10.1016/j.cej.2020.126270.
[14] G. Lama, J. Meijide, A. Sanromán, M. Pazos, Heterogeneous advanced oxidation processes: current approaches for wastewater treatment, Catalysts 12 (2022) 344, https://doi.org/10.3390/catal12030344.
[15] M. Dolatabadi, T. Świergosz, S. Ahmadzadeh, Electro-Fenton approach in oxidative degradation of dimethyl phthalate - the treatment of aqueous leachate from landfills, Sci. Total Environ. 772 (2021) 145323, https://doi.org/10.1016/j.scitotenv.2021.145323.
[16] D. Li, T. Zheng, Y. Liu, D. Hou, K.K. Yao, W. Zhang, H. Song, H. He, W. Shi, L. Wang, J. Ma, A novel Electro-Fenton process characterized by aeration from inside a graphite felt electrode with enhanced electrogeneration of H2O2 and cycle of Fe3+/Fe2+, J. Hazard. Mater. 396 (2020) 122591 https://doi.org/10.1016/j.jhazmat.2020.122591.
[17] D. Li, T. Zheng, Y. Liu, D. Hou, H. He, H. Song, J. Zhang, S. Tian, W. Zhang, L. Wang, J. Ma, A cost-effective Electro-Fenton process with graphite felt electrode aeration for degradation of dimethyl phthalate: enhanced generation of H2O2 and iron recycling that simultaneously regenerates the electrode, Chem. Eng. J. 394 (2020) 125033, https://doi.org/10.1016/j.cej.2020.125033.
[18] R.D.C. Soltani, A. Rezaee, A.R. Khataee, H. Godini, Electrochemical generation of hydrogen peroxide using carbon black-, carbon nanotube-, and carbon black/carbon nanotube-coated gas-diffusion cathodes: effect of operational parameters and decolorization study, Res. Chem. Intermed. 39 (2013) 4277–4286, https://doi.org/10.1007/s11164-012-0944-8.
[19] P.J.M. Cordeiro-Junior, R. Gonçalves, T.T. Guaraldo, R. da Silva Paiva, E. C. Pereira, M.R. de V. Lanza, Oxygen reduction reaction: semi-empirical quantum mechanical and electrochemical study of Printex L6 carbon black, Carbon 156 (2020) 1–9, https://doi.org/10.1016/j.carbon.2019.09.036.
[20] M.S. Kronka, F.L. Silva, A.S. Martins, M.O. Almeida, K.M. Honório, M.R.V. Lanza, Tailoring the ORR selectivity for H2O2 electrogeneration by modification of Printex L6 carbon with 1,4-naphthoquinone: a theoretical, experimental and environmental application study, Mater. Adv. 1 (2020) 1318–1329, https://doi.org/10.1039/D0MA00290A.
[21] G. Gan, X. Li, S. Fan, L. Wang, M. Qin, Z. Yin, G. Chen, Carbon aerogels for environmental clean-up, Eur. J. Inorg. Chem. 2019 (2019) 3126–3141, https://doi.org/10.1002/ejic.201801512.
[22] H. Li, X. Shu, P. Tong, J. Zhang, P. An, Z. Lv, H. Tian, J. Zhang, H. Xia, Fe–Ni alloy nanoclusters anchored on carbon aerogels as high-efficiency oxygen electrocatalysts in rechargeable Zn–air batteries, Small 17 (2021) 2102002, https://doi.org/10.1002/smll.202102002.
[23] J.-M. Liu, Z.-Y. Ji, Y.-B. Shi, P. Yuan, X.-F. Guo, L.-M. Zhao, S.-M. Li, H. Li, J.-S. Yuan, Effective treatment of levofloxacin wastewater by an electro-Fenton process with hydrothermal-activated graphite felt as cathode, Environ. Pollut. 266 (2020) 115348, https://doi.org/10.1016/j.envpol.2020.115348.
[24] H. Nsubuga, C. Basheer, M. Baseer Haider, An enhanced beta-blockers degradation method using copper-boron-ferrite supported graphite electrodes and continuous droplet flow-assisted electro-Fenton reactor, Sep. Purif. Technol. 221 (2019) 408–420, https://doi.org/10.1016/j.seppur.2019.03.095.
[25] H. Qi, X. Sun, Z. Sun, Cu-doped Fe2O3 nanoparticles/etched graphite felt as bifunctional cathode for efficient degradation of sulfamethoxazole in the heterogeneous electro-Fenton process, Chem. Eng. J. 427 (2022) 131695, https://doi.org/10.1016/j.cej.2021.131695.
[26] E. Fajardo-Puerto, A. Elmouwahidi, E. Bailón-García, A.F. Pérez-Cadenas, F. Carrasco-Marín, From Fenton and ORR 2e−-type catalysts to bifunctional electrodes for environmental remediation using the electro-Fenton process, Catalysts 13 (2023) 674, https://doi.org/10.3390/catal13040674.
[27] P.J.M. Cordeiro-Junior, M.S. Kronka, L.A. Goulart, N.C. Veríssimo, L.H. Mascaro, M.C. dos Santos, R. Bertazzoli, M.R. de V. Lanza, Catalysis of oxygen reduction reaction for H2O2 electrogeneration: The impact of different conductive carbon matrices and their physicochemical properties, J. Catal. 392 (2020) 56–68, https://doi.org/10.1016/j.jcat.2020.09.020.
[28] H. Xu, H. Guo, C. Chai, N. Li, X. Lin, W. Xu, Anodized graphite felt as an efficient cathode for in-situ hydrogen peroxide production and Electro-Fenton degradation of rhodamine B, Chemosphere 286 (2022) 131936, https://doi.org/10.1016/j.chemosphere.2021.131936.
[29] W. Yang, M. Zhou, N. Oturan, M. Bechelany, M. Cretin, M.A. Oturan, Highly efficient and stable FeIIFeIII LDH carbon felt cathode for removal of pharmaceutical ofloxacin at neutral pH, J. Hazard. Mater. 393 (2020) 122513, https://doi.org/10.1016/j.jhazmat.2020.122513.
[30] N. Barhoumi, N. Oturan, H. Olvera-Vargas, E. Brillas, A. Gadri, S. Ammar, M. A. Oturan, Pyrite as a sustainable catalyst in electro-Fenton process for improving oxidation of sulfamethazine. Kinetics, mechanism and toxicity assessment, Water Res. 94 (2016) 52–61, https://doi.org/10.1016/j.watres.2016.02.042.
[31] L. Labiadh, M.A. Oturan, M. Panizza, N.B. Hamadi, S. Ammar, Complete removal of AHPS synthetic dye from water using new electro-Fenton oxidation catalyzed by natural pyrite as heterogeneous catalyst, J. Hazard. Mater. 297 (2015) 34–41, https://doi.org/10.1016/j.jhazmat.2015.04.062.
[32] Y. Zhang, M. Gao, S.-G. Wang, W. Zhou, Y. Sang, X.-H. Wang, Integrated electro-Fenton process enabled by a rotating Fe3O4/gas diffusion cathode for simultaneous generation and activation of H2O2, Electrochim. Acta 231 (2017) 694–704, https://doi.org/10.1016/j.electacta.2017.02.091.
[33] L. Cui, H. Huang, P. Ding, S. Zhu, W. Jing, X. Gu, Cogeneration of H2O2 and OH via a novel Fe3O4/MWCNTs composite cathode in a dual-compartment electro-Fenton membrane reactor, Sep. Purif. Technol. 237 (2020) 116380, https://doi.org/10.1016/j.seppur.2019.116380.
[34] X. Shen, F. Xiao, H. Zhao, Y. Chen, C. Fang, R. Xiao, W. Chu, G. Zhao, In situ-formed PdFe nanoalloy and carbon defects in cathode for synergic reduction–oxidation of chlorinated pollutants in electro-Fenton process, Environ. Sci. Technol. 54 (2020) 4564–4572, https://doi.org/10.1021/acs.est.9b05896.
[35] M. Ghasemi, A. Khataee, P. Gholami, R.D.C. Soltani, A. Hassani, Y. Orooji, In-situ electro-generation and activation of hydrogen peroxide using a CuFeNLDH-CNTs modified graphite cathode for degradation of cefazolin, J. Environ. Manage. 267 (2020) 110629, https://doi.org/10.1016/j.jenvman.2020.110629.
[36] Q. Liu, S. Cao, Y. Qiu, Effect of carbonization temperature on bimetallic FeCo-N/C nanofiber electrocatalysts for oxygen reduction reaction in sulfuric acid solution, Int. J. Hydrog. Energy 42 (2017) 29274–29282, https://doi.org/10.1016/j.ijhydene.2017.10.069.
[37] S. Sajjadi, A. Hasanzadeh, A. Khataee, Two-electron oxygen reduction on NiFe alloy enclosed carbonic nanolayers derived from NiFe-metal-organic frameworks, J. Electroanal. Chem. 840 (2019) 449–455, https://doi.org/10.1016/j.jelechem.2019.04.025.
[38] M. Zarei, D. Salari, A. Niaei, A. Khataee, Peroxi-coagulation degradation of C.I. Basic Yellow 2 based on carbon-PTFE and carbon nanotube-PTFE electrodes as cathode, Electrochim. Acta 54 (2009) 6651–6660, https://doi.org/10.1016/j.electacta.2009.06.060.
[39] L. Zhou, Z. Hu, C. Zhang, Z. Bi, T. Jin, M. Zhou, Electrogeneration of hydrogen peroxide for electro-Fenton system by oxygen reduction using chemically modified graphite felt cathode, Sep. Purif. Technol. 111 (2013) 131–136, https://doi.org/10.1016/j.seppur.2013.03.038.
[40] F. Yu, M. Zhou, L. Zhou, R. Peng, A novel electro-Fenton process with H2O2 generation in a rotating disk reactor for organic pollutant degradation, Environ. Sci. Technol. Lett. 1 (2014) 320–324, https://doi.org/10.1021/ez500178p.
[41] F. Xiao, Z. Wang, J. Fan, T. Majima, H. Zhao, G. Zhao, Selective electrocatalytic reduction of oxygen to hydroxyl radicals via 3-electron pathway with FeCo alloy encapsulated carbon aerogel for fast and complete removing pollutants, Angew. Chem. Int. Ed. 60 (2021) 10375–10383, https://doi.org/10.1002/anie.202101804.
[42] Q. Abbas, M. Mirzaeian, M.A. Abdelkareem, A. Al Makky, A. Yadav, A.G. Olabi, Structural tuneability and electrochemical energy storage applications of resorcinol-formaldehyde-based carbon aerogels, Int. J. Energy Res. 46 (2022) 5478–5502, https://doi.org/10.1002/er.7556.
[43] Y. Zhu, F. Deng, S. Qiu, F. Ma, Y. Zheng, L. Gao, A self-sufficient electro-Fenton system with enhanced oxygen transfer for decontamination of pharmaceutical wastewater, Chem. Eng. J. 429 (2022) 132176, https://doi.org/10.1016/j.cej.2021.132176.
[44] E. Rosales, S. Diaz, M. Pazos, M.A. Sanromán, Comprehensive strategy for the degradation of anti-inflammatory drug diclofenac by different advanced oxidation processes, Sep. Purif. Technol. 208 (2019) 130–141, https://doi.org/10.1016/j.seppur.2018.04.014.
[45] Z. Hajalifard, M. Mousazadeh, S. Khademi, N. Khademi, M.H. Jamadi, M. Sillanpää, The efficacious of AOP-based processes in concert with electrocoagulation in abatement of CECs from water/wastewater, npj Clean Water 6 (2023) 1–25, https://doi.org/10.1038/s41545-023-00239-9.
[46] S. Bai, X. Shen, G. Zhu, Z. Xu, J. Yang, In situ growth of FeNi alloy nanoflowers on reduced graphene oxide nanosheets and their magnetic properties, CrstEngComm 14 (2012) 1432–1438, https://doi.org/10.1039/C1CE05916E.

[47] G. Fu, Z. Cui, Y. Chen, Y. Li, Y. Tang, J.B. Goodenough, Ni3Fe-N doped carbon sheets as a bifunctional electrocatalyst for air cathodes, Adv. Energy Mater. 7 (2017) 1601172, https://doi.org/10.1002/aenm.201601172.
[48] J.-W. Zhang, H. Zhang, T.-Z. Ren, Z.-Y. Yuan, T.J. Bandosz, FeNi doped porous carbon as an efficient catalyst for oxygen evolution reaction, Front. Chem. Sci. Eng. 15 (2021) 279–287, https://doi.org/10.1007/s11705-020-1965-2.
[49] J. Hwang, J.-H. Jin, H. Kim, K.Y. Lee, I.-H. Yang, Fabrication of Ni2O3–NiCx core–shell nanoparticles on fluorine-doped tin oxide electrodes via oxygen feeding from SnO2 under hydrogen conditions and their electrochemical performance as supercapacitors, Colloid Interface Sci. Commun. 44 (2021) 100470, https://doi.org/10.1016/j.colcom.2021.100470.
[50] H. Zhao, L. Qian, Y. Chen, Q. Wang, G. Zhao, Selective catalytic two-electron O2 reduction for onsite efficient oxidation reaction in heterogeneous electro-Fenton process, Chem. Eng. J. 332 (2018) 486–498, https://doi.org/10.1016/j.cej.2017.09.093.
[51] K. Liu, J.-C.-C. Yu, H. Dong, J.C.S. Wu, M.R. Hoffmann, Degradation and mineralization of carbamazepine using an electro-Fenton reaction catalyzed by magnetite nanoparticles fixed on an electrocatalytic carbon fiber textile cathode, Environ. Sci. Technol. 52 (2018) 12667–12674, https://doi.org/10.1021/acs.est.8b03916.
[52] K.S.W. Sing, Reporting physisorption data for gas, solid systems with special reference to the determination of surface area and porosity (Recommendations 1984), Pure Appl. Chem. 57 (1985) (1984) 603–619, https://doi.org/10.1351/pac198557040603.
[53] O. Czakkel, K. Marthi, E. Geissler, K. László, Influence of drying on the morphology of resorcinol–formaldehyde-based carbon gels, Microporous Mesoporous Mater. 86 (2005) 124–133, https://doi.org/10.1016/j.micromeso.2005.07.021.
[54] C. Chen, Y. Zhu, M. Tian, Y. Chen, Y. Yang, K. Jiang, S. Gao, Sustainable self-powered electro-Fenton degradation using N, S co-doped porous carbon catalyst fabricated with adsorption-pyrolysis-doping strategy, Nano Energy 81 (2021) 105623, https://doi.org/10.1016/j.nanoen.2020.105623.
[55] R. Bardestani, G.S. Patience, S. Kaliaguine, Experimental methods in chemical engineering: specific surface area and pore size distribution measurements—BET, BJH, and DFT, Can. J. Chem. Eng. 97 (2019) 2781–2791, https://doi.org/10.1002/cjce.23632.
[56] H. Zhao, L. Qian, X. Guan, D. Wu, G. Zhao, Continuous bulk FeCuC aerogel with ultradispersed metal nanoparticles: an efficient 3D heterogeneous Electro-Fenton cathode over a wide range of pH 3–9, Environ. Sci. Technol. 50 (2016) 5225–5233, https://doi.org/10.1021/acs.est.6b00265.
[57] G. Fu, Z. Cui, Y. Chen, L. Xu, Y. Tang, J.B. Goodenough, Hierarchically mesoporous nickel-iron nitride as a cost-efficient and highly durable electrocatalyst for Zn-air battery, Nano Energy 39 (2017) 77–85, https://doi.org/10.1016/j.nanoen.2017.06.029.
[58] A. Abdelwahab, J. Castelo-Quibén, M. Pérez-Cadenas, F.J. Maldonado-Hódar, F. Carrasco-Marín, A.F. Pérez-Cadenas, Insight of the effect of graphitic cluster in the performance of carbon aerogels doped with nickel as electrodes for supercapacitors, Carbon 139 (2018) 888–895, https://doi.org/10.1016/j.carbon.2018.07.034.
[59] F.J. Maldonado-Hódar, C. Moreno-Castilla, J. Rivera-Utrilla, Y. Hanzawa, Y. Yamada, Catalytic graphitization of carbon aerogels by transition metals, Langmuir 16 (2000) 4367–4373, https://doi.org/10.1021/la991080r.
[60] Z. Xu, D. Cai, Z. Hu, L. Gan, A combination of porous and crystalline characters in carbon aerogels by a synergistic graphitization, Microporous Mesoporous Mater. 195 (2014) 36–42, https://doi.org/10.1016/j.micromeso.2014.04.013.
[61] B. Wang, Y. Xia, G. Wang, Y. Zhou, H. Wang, Core shell MoS2/C nanospheres embedded in foam-like carbon sheets composite with an interconnected macroporous structure as stable and high-capacity anodes for sodium ion batteries, Chem. Eng. J. 309 (2017) 417–425, https://doi.org/10.1016/j.cej.2016.10.073.
[62] J. Ding, Q. Sun, L. Zhong, X. Wang, L. Chai, Q. Li, T.-T. Li, Y. Hu, J. Qian, S. Huang, Thermal conversion of hollow nickel-organic framework into bimetallic FeNi3 alloy embedded in carbon materials as efficient oer electrocatalyst, Electrochim. Acta 354 (2020) 136716, https://doi.org/10.1016/j.electacta.2020.136716.
[63] L. Cui, D. Wu, X. Liu, Y. Li, X. Fan, F. Zhang, G. Zhang, W. Peng, Electro-reduction induced fast metal redox cycle on Co3O4-CuO@CNTs/Copper foam cathode for enhanced Fenton-like reaction, J. Colloid Interface Sci. 643 (2023) 613–625, https://doi.org/10.1016/j.jcis.2023.03.145.
[64] Y.J. Sa, J.H. Kim, S.H. Joo, Active edge-site-rich carbon nanocatalysts with enhanced electron transfer for efficient electrochemical hydrogen peroxide production, Angew. Chem. Int. Ed. 58 (2019) 1100–1105, https://doi.org/10.1002/anie.201812435.
[65] A.K. Yousef, Y. Kim, P. Bhanja, P. Mei, M. Pramanik, M.M.S. Sanad, M.M. Rashad, A.Y. El-Sayed, A. Ali Alshehri, Y. Gamaan Alghamdi, K. Ahmed Alzahrani, Y. Ide, J. Lin, Y. Yamauchi, Iron phosphide anchored nanoporous carbon as an efficient electrode for supercapacitors and the oxygen reduction reaction, RSC Adv. 9 (2019) 25240–25247, https://doi.org/10.1039/C9RA04326H.
[66] H. Zhao, X. Shen, Y. Chen, S.-N. Zhang, P. Gao, X. Zhen, X.-H. Li, G. Zhao, A COOH-terminated nitrogen-doped carbon aerogel as a bulk electrode for completely selective two-electron oxygen reduction to H2O2, Chem. Commun. 55 (2019) 6173–6176, https://doi.org/10.1039/C9CC02580D.
[67] K.-H. Wu, D. Wang, X. Lu, X. Zhang, Z. Xie, Y. Liu, B.-J. Su, J.-M. Chen, D.-S. Su, W. Qi, S. Guo, Highly selective hydrogen peroxide electrosynthesis on carbon: In situ interface engineering with surfactants, Chem 6 (2020) 1443–1458, https://doi.org/10.1016/j.chempr.2020.04.002.
[68] X. Xiao, S. Peng, C. Wang, D. Cheng, N. Li, Y. Dong, Q. Li, D. Wei, P. Liu, Z. Xie, D. Qu, X. Li, Metal/metal oxide@carbon composites derived from bimetallic Cu/Ni-based MOF and their electrocatalytic performance for glucose sensing, J. Electroanal. Chem. 841 (2019) 94–100, https://doi.org/10.1016/j.jelechem.2019.04.038.
[69] Y. Meng, T.M. Young, P. Liu, C.I. Contescu, B. Huang, S. Wang, Ultralight carbon aerogel from nanocellulose as a highly selective oil absorption material, Cellul. 22 (2015) 435–447, https://doi.org/10.1007/s10570-014-0519-5.
[70] H.A. Kuo, A. Ramachandran, D.I. Oyarzun, E.C. Clevenger, J.G. Santiago, M. Stadermann, P.G. Campbell, S.A. Hawks, Understanding resistances in capacitive deionization devices, Environ. Sci. Water Res. Technol. 6 (2020) 1842–1854, https://doi.org/10.1039/D0EW00169D.
[71] M. Shi, Y. Chen, H. Wen, Y. Liu, One-step heat treatment to process semi-coke powders as an anode material with superior rate performance for Li-ion batteries, RSC Adv. 8 (2018) 41207–41217, https://doi.org/10.1039/C8RA07899H.
[72] P. Chen, K. Xu, T. Zhou, Y. Tong, J. Wu, H. Cheng, X. Lu, H. Ding, C. Wu, Y. Xie, Strong-coupled cobalt borate nanosheets/graphene hybrid as electrocatalyst for water oxidation under both alkaline and neutral conditions, Angew. Chem. Int. Ed. 55 (2016) 2488–2492, https://doi.org/10.1002/anie.201511032.
[73] I. Diouf, O. Dia, M.B. Diedhiou, P. Drogui, A.O. Toure, S.M. Lo, M. Rumeau, C. G. Mar/Diop, Electro-generation of hydrogen peroxide using a graphite cathode from exhausted batteries: study of influential parameters on electro-Fenton process, Environ. Technol. 41 (2020) 1434–1445, https://doi.org/10.1080/09593330.2018.1537309.
[74] Y. Fu, H.-Y. Yu, C. Jiang, T.-H. Zhang, R. Zhan, X. Li, J.-F. Li, J.-H. Tian, R. Yang, NiCo alloy nanoparticles decorated on N-doped carbon nanofibers as highly active and durable oxygen electrocatalyst, Adv. Funct. Mater. 28 (2018) 1705094, https://doi.org/10.1002/adfm.201705094.
[75] Z. Li, X. Xu, X. Lu, C. He, J. Huang, W. Sun, L. Tian, Synergistic coupling of FeNi3 alloy with graphene carbon dots for advanced oxygen evolution reaction electrocatalysis, J. Colloid Interface Sci. 615 (2022) 273–281, https://doi.org/10.1016/j.jcis.2022.01.088.
[76] Business Electricity Rates UK, Bus. Electr. Prices (n.d.). https://www.businesselectricityprices.org.uk/ (accessed May 14, 2024).
[77] F.E. Titchou, H. Zazou, H. Afanga, E.G. Jamila, R. Ait Akbour, M. Hamdani, M. A. Oturan, Comparative study of the removal of direct red 23 by anodic oxidation, electro-Fenton, photo-anodic oxidation and photoelectro-Fenton in chloride and sulfate media, Environ. Res. 204 (2022) 112353, https://doi.org/10.1016/j.envres.2021.112353.
[78] Q. Ye, H. Xu, Q. Wang, X. Huo, Y. Wang, X. Huang, G. Zhou, J. Lu, J. Zhang, New insights into the mechanisms of tartaric acid enhancing homogeneous and heterogeneous copper-catalyzed Fenton-like systems, J. Hazard. Mater. 407 (2021) 124351, https://doi.org/10.1016/j.jhazmat.2020.124351.
[79] Q. Ye, H. Xu, J. Zhang, Q. Wang, P. Zhou, Y. Wang, X. Huang, X. Huo, C. Liu, J. Lu, Enhancement of peroxymonosulfate activation for antibiotics removal by nano zero valent tungsten induced Cu(II)/Cu(I) redox cycles, Chem. Eng. J. 382 (2020) 123054, https://doi.org/10.1016/j.cej.2019.123054.
[80] X. Qin, P. Cao, X. Quan, K. Zhao, S. Chen, H. Yu, Y. Su, Highly efficient hydroxyl radicals production boosted by the atomically dispersed Fe and Co sites for heterogeneous electro-Fenton oxidation, Environ. Sci. Technol. 57 (2023) 2907–2917, https://doi.org/10.1021/acs.est.2c06981.
[81] Y. Yao, Y. Pan, Y. Yu, Z. Yu, L. Lai, F. Liu, L. Wei, Y. Chen, Bifunctional catalysts for heterogeneous electro-Fenton processes: a review, Environ. Chem. Lett. 20 (2022) 3837–3859, https://doi.org/10.1007/s10311-022-01453-6.
[82] J. Xie, C. Zhang, T.D. Waite, Hydroxyl radicals in anodic oxidation systems: generation, identification and quantification, Water Res. 217 (2022) 118425, https://doi.org/10.1016/j.watres.2022.118425.
[83] H. Zhang, X. Wan, G. Li, F. Zhang, A three-electrode electro-fenton system supplied by self-generated oxygen with automatic pH-regulation for groundwater remediation, Electrochim. Acta 250 (2017) 42–48, https://doi.org/10.1016/j.electacta.2017.08.040.
[84] J. Zhang, Y. Liu, J. Li, K. Wang, X. Zhao, X. Liu, Enhanced recovery of phosphorus from hypophosphite-laden wastewater via field-induced electro-Fenton coupled with anodic oxidation, J. Hazard. Mater. 464 (2024) 132750, https://doi.org/10.1016/j.jhazmat.2023.132750.
[85] S.Y. Yang, H.W. Jeong, B. Kim, D.S. Han, W. Choi, H. Park, Electrocatalytic cogeneration of reactive oxygen species for synergistic water treatment, Chem. Eng. J. 358 (2019) 497–503, https://doi.org/10.1016/j.cej.2018.09.192.
[86] F. Yu, M. Zhou, X. Yu, Cost-effective electro-Fenton using modified graphite felt that dramatically enhanced on H2O2 electro-generation without external aeration, Electrochim. Acta 163 (2015) 182–189, https://doi.org/10.1016/j.electacta.2015.02.166.
[87] A.R. Khataee, M. Safarpour, M. Zarei, S. Aber, Electrochemical generation of H2O2 using immobilized carbon nanotubes on graphite electrode fed with air: investigation of operational parameters, J. Electroanal. Chem. 659 (2011) 63–68, https://doi.org/10.1016/j.jelechem.2011.05.002.
[88] F. Qiu, L. Wang, H. Li, Y. Pan, H. Song, J. Chen, Y. Fan, S. Zhang, Electrochemically enhanced activation of Co3O4/TiO2 nanotube array anode for persulfate toward high catalytic activity, low energy consumption, and long lifespan performance, J. Colloid Interface Sci. 655 (2024) 594–610, https://doi.org/10.1016/j.jcis.2023.11.045.
[89] S. Cheng, C. Shen, H. Zheng, F. Liu, A. Li, OCNTs encapsulating Fe-Co PBA as efficient chainmail-like electrocatalyst for enhanced heterogeneous electro-Fenton reaction, Appl. Catal. B Environ. 269 (2020) 118785, https://doi.org/10.1016/j.apcatb.2020.118785.

[90] J. Ekspong, E. Gracia-Espino, T. Wågberg, Hydrogen evolution reaction activity of heterogeneous materials: a theoretical model, J. Phys. Chem. C 124 (2020) 20911–20921, https://doi.org/10.1021/acs.jpcc.0c05243.
[91] J. He, X. Yang, B. Men, D. Wang, Interfacial mechanisms of heterogeneous Fenton reactions catalyzed by iron-based materials: a review, J. Environ. Sci. 39 (2016) 97–109, https://doi.org/10.1016/j.jes.2015.12.003.
[92] M. Qutob, M.A. Hussein, K.A. Alamry, M. Rafatullah, A review on the degradation of acetaminophen by advanced oxidation process: pathway, by-products, biotoxicity, and density functional theory calculation, RSC Adv. 12 (2022) 18373–18396, https://doi.org/10.1039/D2RA02469A.
[93] S. Chen, P. He, P. Zhou, X. Wang, F. Xiao, Q. He, J. Li, L. Jia, H. Zhang, B. Jia, B. Tang, Development of a novel graphitic carbon nitride and multiwall carbon nanotube co-doped Ti/PbO2 anode for electrocatalytic degradation of acetaminophen, Chemosphere 271 (2021) 129830, https://doi.org/10.1016/j.chemosphere.2021.129830.
[94] Y. Gao, J. Zhou, Y. Rao, H. Ning, J. Zhang, J. Shi, N. Gao, Comparative study of degradation of ketoprofen and paracetamol by ultrasonic irradiation: mechanism, toxicity and DBP formation, Ultrason. Sonochem. 82 (2022) 105906, https://doi.org/10.1016/j.ultsonch.2021.105906.
[95] H. Olvera-Vargas, J.-C. Rouch, C. Coetsier, M. Cretin, C. Causserand, Dynamic cross-flow electro-Fenton process coupled to anodic oxidation for wastewater treatment: application to the degradation of acetaminophen, Sep. Purif. Technol. 203 (2018) 143–151, https://doi.org/10.1016/j.seppur.2018.03.063.
[96] M.D.G. de Luna, M.L. Veciana, C.-C. Su, M.-C. Lu, Acetaminophen degradation by electro-Fenton and photoelectro-Fenton using a double cathode electrochemical cell, J. Hazard. Mater. 217–218 (2012) 200–207, https://doi.org/10.1016/j.jhazmat.2012.03.018.
[97] Y. Ling, G. Liao, P. Xu, L. Li, Fast mineralization of acetaminophen by highly dispersed Ag-g-C3N4 hybrid assisted photocatalytic ozonation, Sep. Purif. Technol. 216 (2019) 1–8, https://doi.org/10.1016/j.seppur.2019.01.057.
[98] S.O. Ganiyu, N. Oturan, S. Raffy, M. Cretin, C. Causserand, M.A. Oturan, Efficiency of plasma elaborated sub-stoichiometric titanium oxide (Ti4O7) ceramic electrode for advanced electrochemical degradation of paracetamol in different electrolyte media, Sep. Purif. Technol. 208 (2019) 142–152, https://doi.org/10.1016/j.seppur.2018.03.076.
[99] T.X.H. Le, T.V. Nguyen, Z. Amadou Yacouba, L. Zoungrana, F. Avril, D.L. Nguyen, E. Petit, J. Mendret, V. Bonniol, M. Bechelany, S. Lacour, G. Lesage, M. Cretin, Correlation between degradation pathway and toxicity of acetaminophen and its by-products by using the electro-Fenton process in aqueous media, Chemosphere 172 (2017) 1–9, https://doi.org/10.1016/j.chemosphere.2016.12.060.
[100] F. Ghanbari, A. Hassani, S. Wacławek, Z. Wang, G. Matyszczak, K.-Y.-A. Lin, M. Dolatabadi, Insights into paracetamol degradation in aqueous solutions by ultrasound-assisted heterogeneous electro-Fenton process: Key operating parameters, mineralization and toxicity assessment, Sep. Purif. Technol. 266 (2021) 118533, https://doi.org/10.1016/j.seppur.2021.118533.
[101] C. Xue, Z. Cao, X. Tong, P. Yang, S. Li, X. Chen, D. Liu, W. Huang, Investigation of CuCoFe-LDH as an efficient and stable catalyst for the degradation of acetaminophen in heterogeneous electro-Fenton system: Key operating parameters, mechanisms and pathways, J. Environ. Manage. 327 (2023) 116787, https://doi.org/10.1016/j.jenvman.2022.116787.
[102] H. Öztürk, S. Barışçı, O. Turkay, Paracetamol degradation and kinetics by advanced oxidation processes (AOPs): Electro-peroxone, ozonation, goethite catalyzed electro-fenton and electro-oxidation, Environ. Eng. Res. 26 (2021), https://doi.org/10.4491/eer.2018.332.
[103] S. Ahmadzadeh, M. Dolatabadi, Removal of acetaminophen from hospital wastewater using electro-Fenton process, Environ. Earth Sci. 77 (2018) 53, https://doi.org/10.1007/s12665-017-7203-7.
[104] L.C. Almeida, S. Garcia-Segura, N. Bocchi, E. Brillas, Solar photoelectro-Fenton degradation of paracetamol using a flow plant with a Pt/air-diffusion cell coupled with a compound parabolic collector: Process optimization by response surface methodology, Appl. Catal. B Environ. 103 (2011) 21–30, https://doi.org/10.1016/j.apcatb.2011.01.003.